Climate
Impact Lab

Documentation for

Data-driven Spatial Climate Impact Model (DSCIM)

Version092022-EPA

The Climate Impact Lab

September 2022

Contents

1 Background **1**

2 Socioeconomics and Emissions Module **2**

2.1 Historical income data 2

2.2 Future income, population, and emissions projections 3

3 Climate Module **4**

3.1 High resolution data and simulations 5

3.1.1 Historical climate data 5

3.1.2 Future climate simulations 5

3.2 SC-GHG simulations using the FaIR climate model emulator 7

4 Damages Module **10**

4.1 Dose response function estimation and projection 10

4.1.1 Estimation 10

4.1.2 Projections 11

4.2 Damage function estimation 15

4.3 Calculation of probabilistic damage streams using FaIR climate outputs 17

5 Discounting Module & Valuation **19**

5.1 Discounting Procedure 19

5.2 The Weitzman parameter 19

6 Putting it all together: the SC-GHG calculation **20**

6.1 Step by step process to SC-GHGs 20

6.2 DSCIM-EPA user options and defaults 24

A Appendix: Accounting for risk aversion **26**

A.1 The certainty equivalent 26

A.2 Illustration of risk averse damage function 26

B Appendix: Damage Function Emulation **29**

C Appendix: Sector-specific Damages Details **31**

C.1 Mortality 31

C.2 Energy 32

C.3 Labor Supply 34

C.4 Agricultural Productivity 35

C.5 Coastal 38

Abbreviations

ADM1	First Administrative Division Level (e.g., state/province)
AEO	Annual Energy Outlook
BCSD	Bias Correction and Spatial Disaggregation
BEST	Berkeley Earth Surface Temperature
CE	Certainty Equivalent
CIAM	Coastal Impact and Adaptation Model
CIL	Climate Impact Lab
CMIP	Coupled Model Intercomparison Project
DSCIM	Data-driven Spatial Climate Impact Model
ECS	Equilibrium Climate Sensitivity
EPA	Environmental Protection Agency
ESL	Extreme Sea Level
FACTS	Framework for Assessing Changes to Sea-level
FaIR	Finite Amplitude Impulse Response model
GCM	Global Climate Model
GDDP	Global Daily Downscaled Projections
GDP	Gross Domestic Product
GHG	Greenhouse Gases
GMFD	Global Meteorological Forcing Dataset
GMST	Global Mean Surface Temperature
GMSL	Global Mean Sea Level
IAM	Integrated Assessment Model
IAV	Impacts, Adaptation, and Vulnerability
IEA	International Energy Agency
IIASA	International Institute for Applied Systems Analysis
IPCC	Intergovernmental Panel on Climate Change
LMSL	Local Mean Sea Level
NASEM	National Academies of Sciences, Engineering, and Medicine
NEX	NASA Earth Exchange
OECD	Organization for Economic Cooperation and Development
PPP	Purchasing Power Parity
PWT	Penn World Tables
RCP	Representative Concentration Pathway

Abbreviations contd.

RFF	Resources for the Future
RIA	Regulatory Impact Analysis
SCC	Social Cost of Carbon
SC-GHG	Social Cost of Greenhouse Gases
SESL	Semi-Empirical Sea Level
SLR	Sea level Rise
SMME	Surrogate Model Mixed Ensemble
SP	Müller-Stock-Watson-RFF Socioeconomic Projections
SSP	Shared Socioeconomic Pathway
TCR	Transient Climate Response
UDEL	University of Delaware
VSL	Value of a Statistical Life

1 Background

Rapid advancement in both climate science and economics over the last decade means there is an urgent need to update the social cost of carbon and other greenhouse gases (collectively referred to as SC-GHGs), as called for in both the 2017 National Academies of Sciences, Engineering, and Medicine (NASEM) report, "Valuing Climate Damages," (*1*) and the January 2021 Executive Order 13990, "Protecting Public Health and the Environment and Restoring Science to Tackle the Climate Crisis." Updating U.S. SC-GHG estimates based on the recommendations of NASEM would return them to the frontier of understanding about the risks from climate change (*2*).

The Climate Impact Lab (CIL) has developed the Data-driven Spatial Climate Impact Model (DSCIM), a robust, empirically-based model for estimating SC-GHGs that is grounded in the best available science and economics and is consistent with recommendations set out by the NASEM (*1*). The theory, framework, and implementation of the CIL's complete approach has been peer-reviewed and is published in *Nature* (*3*) and *The Quarterly Journal of Economics* (*4*), with many technical elements, including the construction of empirical damage functions and valuation of uncertain and unequal local impacts, published in our earlier 2017 *Science* article (*5*). In this user manual, we provide an overview of the key components of an implementation of DSCIM, referred to as DSCIM-EPA, for the U.S. Environmental Protection Agency's (EPA) September 2022 draft technical report, "Report on the Social Cost of Greenhouse Gases: Estimates Incorporating Recent Scientific Advances."

DSCIM-EPA contains four major components, each of which is based on best-available science and has been detailed in our peer-reviewed publications (*3*, *4*, *5*):

1. Socioeconomics and emissions projections DSCIM-EPA produces SC-GHGs that are consistent with the NASEM recommendations, employing the Resources for the Future Socioeconomic Projections (RFF-SPs). These provide probabilistic, country-level projections of population, GDP, and greenhouse gas emissions, while allowing for some dependencies among individual scenario draws in each dimension. Further detail can be found in Section 2.

2. Climate System Representation DSCIM-EPA incorporates the Finite Amplitude Impulse Response (FaIR) model, which was identified by the NASEM as a simple climate model capable of meeting key criteria related to the current scientific understanding of the timescales on which the climate system responds to CO_2 emissions and of climate-carbon cycle feedbacks (*1*). In Section 3, we outline our implementation of FaIR, to project the impact that an additional ton of CO_2 or other GHG has on global mean surface temperature (GMST).

3. Damage Functions In Section 4, we outline our approach to generating damage functions that are empirically derived and plausibly causal, capture local-level nonlinearities for the entire global population, and are inclusive of both adaptation costs and benefits.

4. Discounting In Section 5, we outline DSCIM-EPA's approach to discounting, supported by the latest empirical evidence and able to capture uncertainty in future growth, as well as the insurance value of climate mitigation that protects against lower probability, higher damage scenarios.

DSCIM will be an evolving model, continuously updated with new sectors and the latest advances in science and economics. The DSCIM-EPA codebase for download and replication of SC-GHG values used by EPA is available online at: https://github.com/ClimateImpactLab/dscim-epa.

2 Socioeconomics and Emissions Module

2.1 Historical income data

One of the most important measures of vulnerability to weather and climate in our analyses is the wealth or incomes of those affected. This means that, in order to capture the differential vulnerability to climate change in our empirical estimates, we need detailed subnational measures of income. In order to obtain income data for each subnational region in the empirical analyses detailed in Section 4, we draw subnational incomes from three main sources, using a combination of subnational gross domestic product (GDP) datasets as well as globally-comprehensive national GDP data.

- **Penn World Tables (PWT) national GDP**.[1] This dataset provides national-level incomes from 1950 to 2014 for most countries in the world. We use Penn World Tables version 9.0 to obtain national-level income for all countries in our analyses.
- **European Union subnational GDP**.[2] This dataset provides national and subnational level income data for the European Union (EU) countries in our datasets. We use this dataset to obtain subnational income at the Nomencalture of Territorial Units for Statistics (NUTS2) level of aggregation.[3]
- **First administrative division (ADM1) subnational GDP from national sources (*6*)**. This dataset provides national and subnational income data for 1,503 administrative regions from 83 countries. We use this dataset to obtain subnational level income data for all countries outside the EU.

Using these data, we construct a consistent multi-country panel of subnational incomes at the NUTS2 level for EU countries and ADM1 level for non-EU countries. To do so, we use the Eurostat (*7*) and

[1] Penn World Tables (PWT) database: https://www.rug.nl/ggdc/productivity/pwt/.
[2] Eurostat database: http://ec.europa.eu/eurostat/data/database.
[3] These data are used only in the mortality analysis detailed in Section C.1.

Gennaioli et al. (*6*) to downscale the PWT national-level incomes. We prefer this approach to using the subnational data directly, as there are known inconsistencies in measurement of subnational GDP across countries. Thus, we make the assumption that the within-country distributions of GDP in the Eurostat and Gennaioli et al. are accurate, but the exact levels may not be. We rely on the PWT data as a consistent measure of GDP levels for all countries; thus, our subnational GDP estimates sum to national GDP from PWT for all countries in the sample. All subnational income data are in constant 2005 dollars purchasing power parity (PPP).

Subnational data collected by reference (*6*) are drawn from disparate sources, often using census data, which are typically not annual, leading to an unbalanced panel. To construct annual values of income per capita using these data, we linearly interpolate between years, before constructing the Bartlett kernel[4] and taking averages across all years. Full details of our construction of these data are provided in reference (*4*).

2.2 Future income, population, and emissions projections

In order to understand the economic impact of climate change in the future, we need to understand what the economy will be like in the future. A standard approach to date has been to project future incomes and populations in multiple different scenarios or pathways, for example in the widely-used shared socioeconomic pathways (SSPs) (*8*). However, this often ignores the probability of the realization of any scenario, and this probability of economic outcomes is essential for characterizing the uncertainty of SC-GHGs. To remedy the challenges of such an approach, RFF have produced a set of 10,000 probabilistic projections of GDP, population, and greenhouse gas emissions scenarios up to year 2300 that we employ in this analysis. These socioeconomic projections (RFF-SPs) are intended to fully meet the criteria of the NASEM report, which notes that purely statistical approaches may not fully inform future growth and should be combined with expert judgement (*1*).

One major advantage of the RFF-SPs is that they establish a set of dependencies across GDP, population, and emissions projections. For example, in a high economic growth projection, this may be associated with technological improvements that could lower emissions intensity of GDP, and therefore be associated with a lower emissions scenario. This correspondence is described more below. The data in the RFF-SPs are provided in 5-year increments. To construct annual estimates, we linearly interpolate between the time-series data in the RFF-SPs in log space for population and GDP at the global-level.

Future projections of GDP. For projections of GDP, RFF combine an econometric approach described in Müller, Stock, and Watson (*9*) with expert elicitation from 10 notable scholars of growth. This approach is fully described in Rennert et al. (*10*). The Müller, Stock, and Watson projections calculate values for 113 countries, and RFF imputes values for a further 71 countries from these in order to have country-level projections for every country represented in the SSP database. The resulting median of GDP per capita

[4]The Bartlett kernel is a method of weighting the time series such that greater weight is given to more recent years.

growth rates varies between approximately 1-1.5 percent annually from 2020 to 2300, with a 1st and 99th range of approximately 0-4 percent.[5]

Future projections of national populations. Population projections build upon the standard methodology employed by the United Nations for population projections up to 2100. In the RFF-SPs, RFF extend this time-horizon to 2300 and combine the statistical methods with expert judgement from 9 leading demographers. Methods and results are fully described in Raftery and Ševčíková (*11*). Median projections generate a population of approximately 11 billion in 2100 and 7.5 billion in 2300.

Future projections of CO_2 emissions A standard approach to date to model future climate based on greenhouse gas emissions has been to use emissions pathways called Representative Concentration Pathways (RCPs) developed for the Coupled Model Intercomparison Projects (CMIP). Rather than follow a purely scenario-based approach like that of the RCPs, RFF produced a distribution of future possible emissions trajectories based on expert elicitation (*10*). These values are then used to establish distributions of future global emissions conditional on five different scenarios of GDP growth. In order to pair socioeconomic simulations with emissions simulations, each randomly drawn economic simulation is associated with a randomly drawn percentile of the emissions distribution for that level of GDP. Across all emissions scenarios, the median trajectory represents a 50 percent decrease in CO_2 emissions in 2100 from today's level.

3 Climate Module

We aim to represent the climate system at the spatial and temporal resolution required to estimate empirical damage functions, allowing for a baseline climate under some assumed trajectory of greenhouse gas emissions to be established, as well as representation of a response to a marginal emission of a greenhouse gas. Because the CIL approach derives global estimates of climate damages by calculating high-resolution, local impact projections, the climate module must be broken into two separate but related components: *(i)* highly spatially and temporally resolved historical climate data, and future climate projections from an ensemble of global climate models (GCMs) combined with surrogate climate models under a range of emissions pathways, which can be used to estimate spatially resolved damages and construct empirically derived global damage functions; and *(ii)* projections of GMST and global mean sea level (GMSL) under a baseline climate and in response to a marginal emission of GHG, including representation of the full probability distribution of climate uncertainty with a large ensemble of simulations.[6]

[5]The RFF-SP GDP is in units of $2011. We convert to $2019 using 1.1346350337995368, which was obtained from the FRED implicit GDP deflator, downloaded circa July 2020.

[6]In principle, one could compute a SC-GHG estimate by perturbing each GCM in the suite with a marginal emission of the greenhouse gas and projecting damages for each location in both the original and perturbed simulations. However, in practice, such a procedure would prevent the calculation of an SC-GHG for any climate trajectory that did not exactly coincide with one of the GCMs, and would also be prohibitively costly from a computational standpoint. Instead, we rely on a probabilistic, reduced-complexity climate-carbon cycle model, in combination with our empirically derived damage functions, to construct

3.1 High resolution data and simulations

To create damage estimates at a highly resolved spatial and temporal resolution, historical climate data and future climate data for multiple emissions scenarios at a high spatial and temporal resolution are required. Historical climate data are used to estimate the relationship between temperature and impacts (called "dose response" functions and described in Section 4.1) within a sector (e.g. the mortality-temperature relationship), and projected future climate data are used to produce climate change damage estimates under several possible emissions trajectories. In the next two sections, historical climate data sources are outlined, followed by a description of the climate change projection data used and how probabilistic weights are assigned to each future climate projection from each GCM in the surrogate model mixed ensemble (SMME), whose method is described in (*12*).

3.1.1 Historical climate data

The primary historical climate data product used is the Global Meteorological Forcing Dataset (GMFD, (*13*)), which includes daily, global, gridded estimates of meteorological variables at the surface. GMFD was derived from a weather forecasting reanalysis product (NCEP/NCAR), allowing for global coverage where observations do not exist and corrected to observational weather data where available. GMFD data is available at a 1/4 degree (about 25 km) horizontal resolution on a daily timescale from 1948-2010. Daily surface temperature and daily total precipitation were used from GMFD. Several other historical climate data sources were used on a sector-by-sector basis to investigate and ensure the consistency of estimated response surfaces across differing climate datasets (Appendix C and references therein).

3.1.2 Future climate simulations

A global high-resolution (1/4 degree, daily) dataset of bias-corrected future climate projections produced by NASA's Earth Exchange program (NEX) is used, called the Global Daily Downscaled Projections (GDDP, (*14*)). This dataset includes projections that are bias corrected and downscaled from the output of 21 GCMs that are part of the Phase 5 CMIP (CMIP5) archive (*15*). The NEX-GDDP dataset was adjusted by NASA using the Bias Correction Spatial Disaggregation (BCSD) statistical downscaling method, which uses as a reference daily maximum and minimum temperature and daily precipitation data from GMFD (1950-2005) and a traditional quantile mapping bias correction approach (*16*, *14*). Quantile mapping is used to adjust the GCM outputs for historical and future time periods, and then the bias-corrected output is spatially downscaled to a 1/4-degree resolution using a delta method that interpolates the daily bias corrected changes relative to the GMFD climatology. For each GCM, three datasets are used: 1) simulated response to historical climate forcing from 1850-2005, 2) simulated response to climate forcing through 2100 under RCP4.5 projected emissions from CMIP5, and 3) under RCP8.5 projected emissions from CMIP5.

SC-GHG estimates, consistent with the recommendations of the NASEM.

Each sector requires a different climate variable transformation, but all are derived from daily maximum and minimum temperature and/or daily total precipitation. When necessary, daily average temperature is taken as the mean of daily maximum and minimum temperatures.

Because the CMIP5 ensemble of GCMs is not representative of a probabilistic distribution of climate uncertainty but instead is an "ensemble of opportunity", it fails to adequately represent tail outcomes. Consequently, we use the SMME method (*12*) to assign probabilistic weights to the GCM climate projections and synthesize "surrogate" GCMs to improve representation of the tails of the distribution. To accomplish this, the SMME approach uses a weighting scheme that is based on projections of GMST from a reduced-complexity climate model and a form of linear pattern scaling to construct model surrogates to fill in the tails of the probability distribution that are not fully represented by the CMIP5 GCMs. The SMME approach provides an additional 12 surrogate models (Figure 1) to the existing 21 NEX-GDDP GCMs. For more on this, see Appendix B.2.3 of (*4*).

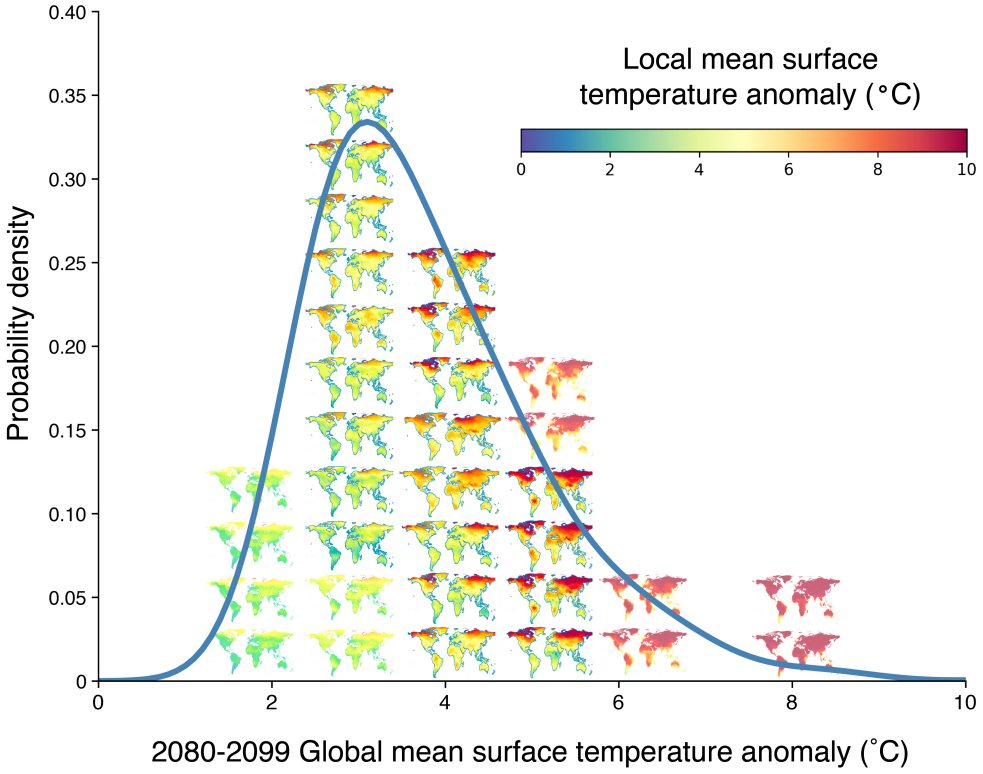

Figure 1: Future climate projections from the surrogate model mixed ensemble (SMME) Figure shows the 21 climate models (outlined maps) and 12 model surrogates (maps without outlines) that are weighted such that the weighted distribution of the 2080 to 2099 global mean surface temperature anomaly (ΔGMST) exhibited by the 33 total models matches the probability distribution of estimated ΔGMST responses (blue-grey line) under RCP8.5. For this construction, the anomaly is relative to the 1986-2005 average.

3.2 SC-GHG simulations using the FaIR climate model emulator

The climate module of an SC-GHG calculation is meant to represent the climate response to the outputs of the socioeconomic module, namely, emissions of greenhouse gases and other forcing agents, such that a baseline climate and response to a marginal emission (or, "pulse") of GHG emissions – CO_2, methane (CH_4), and nitrous oxide (N_2O) in DSCIM-EPA – can be established. The steps for producing simulations necessary for SC-GHG calculations, described in this section, are identical across gases except for the gas species and size of the pulse (see Table 1). To represent the climate response with and without a pulse of emissions, the module must convert the GHG emissions to atmospheric GHG concentrations, and in turn to radiative forcing (how much the energy imbalance is perturbed by the additional greenhouse gas), and finally a global average temperature response to that radiative forcing. The Finite Amplitude Impulse Response (FaIR) reduced-complexity climate model(*17*, *18*) used extensively in the IPCC's 6th Assessment Report (AR6)(*19*), satisfies key criteria for such a module, including those outlined by NASEM (*1*), and was identified by NASEM as an exemplar of a simple climate model meeting those criteria. These criteria include transparency, simplicity, and ability to accurately and probabilistically represent climate and carbon cycle systems and their uncertainties in a manner consistent with IPCC assessments and insights from more complex Earth system models.

We use FaIR version 1.6.2[7] to be consistent with the version used in AR6 Working Group I (WG1) and Working Group III (WG3) reports. To represent the possible set of future climate change, we sample from the set of 10,000 probabilistic emissions pathways from Resources for the Future that, together with probabilistic trajectories of GDP and population, are referred to here as RFF-SPs (*10*) and described in Section 2. Each RFF-SP represents a possible future trajectory of GDP, population, and emissions of CO_2, CH_4, and N_2O, representing a wide range of emissions and climatic pathways (see the top row of Figure 2). Following the method used in previous estimates of SC-GHGs (*1*), projections start in the current period (here defined as 2020) and run through the year 2300.

The SC-GHGs are estimates of the cost to society of emitting a marginal tonne of the GHG. The RFF-SPs represent a probabilistic set of baseline, or "control", climate change scenarios, whereas to represent a set of "pulse" scenarios, a pulse of a GHG emission is added to each of the RFF-SPs in the specified pulse year. The difference between the pulse and control simulations characterizes the climate response to a pulse of GHG emissions. Table 1 lists the pulse sizes for each GHG estimated in DSCIM-EPA – CO_2, CH_4, and N_2O – in gas species units and as entered into the FaIR model emissions array[8]. Pulse years evaluated are: 2020, 2030, 2040, 2050, 2060, 2070, and 2080.

[7] https://github.com/OMS-NetZero/FAIR/tree/v1.6.2

[8] FaIR expects an emissions array of 39 different species, 3 of which are included in the RFF-SPs. Emissions for other gases and for the time range outside of 2020-2300 are taken from the CMIP6 SSP2-4.5 emissions pathway as provided by the Reduced Complexity Model Intercomparison Project (www.rcmip.org), which includes historical emissions for past years. These emissions are concatenated with the RFF-SPs in order to run FaIR from 1750-2500 but are otherwise trimmed to 2020-2300 for the SC-GHG calculations.

[9] https://www.rcmip.org/

GHG	Pulse size (species units)	Pulse size (FaIR input)
CO_2	3.66 Gt CO_2	1.0 GtC
CH_4	40.0 Mt CH_4	40.0 Mt CH_4
N_2O	1.57 Mt N_2O	1.0 Mt N_2

Table 1: Pulse sizes were chosen to be approximately 10% of year 2020 emissions for each gas. The reference 2020 emissions were taken from the globally aggregated SSP3-7.0 emissions produced for the Reduced Complexity Model Intercomparison Project (RCMIP)[9]. SSP3-7.0 is a standard emissions pathway from CMIP6. "Mt‘ is Megatonne,

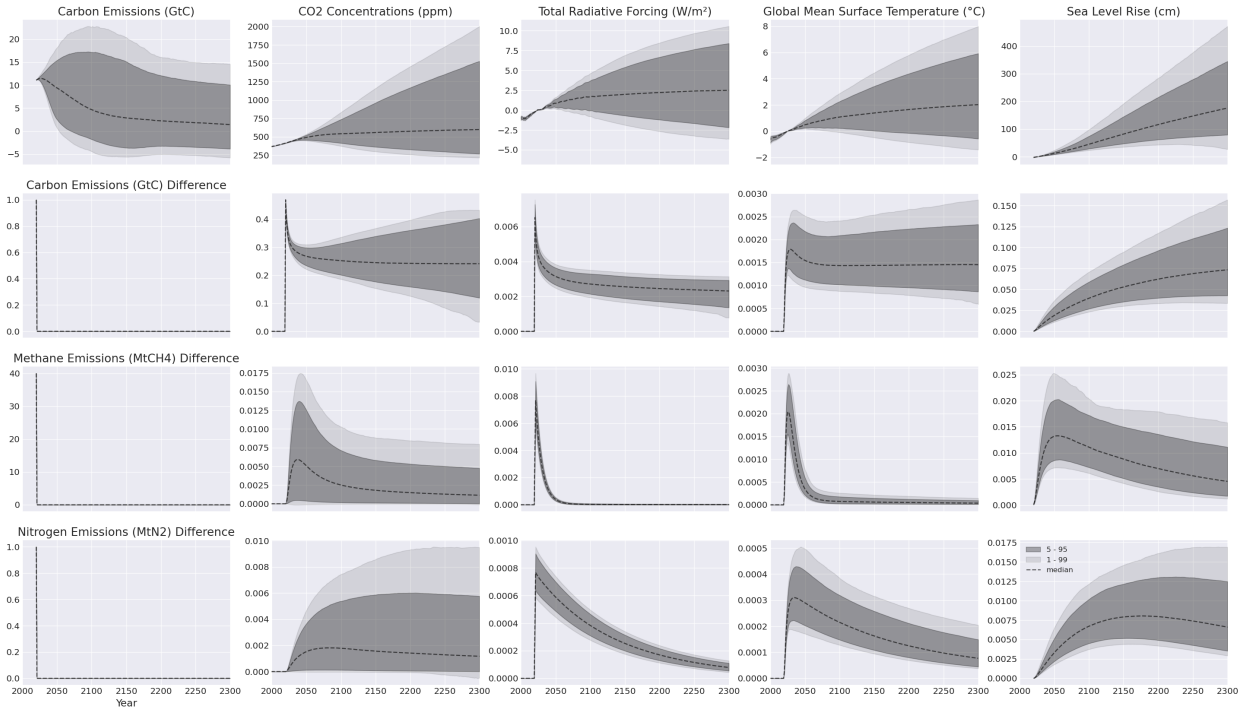

Figure 2: Baseline and difference between the pulse and baseline for key climate variables in the FaIR simple climate model: Each panel shows the temporal trajectory of key variables in FaIR that underlie our calculation of the SC-GHGs. All panels show percentiles (1-99 range, light gray shading; 5-95 range, dark gray shading; median, dashed curve) across the 10,000 RFF-SP-FaIR climate parameter draws. **Row one**) RFF-SP emissions (column one) and the response to the RFF-SP emissions. These constitute the baseline ("control") simulations. The RFF-SPs include CO_2 , CH_4, and N_2O emissions trajectories, but only CO_2 baseline emissions in units of gigatonnes of carbon (GtC) are shown here (top row, first column). The values for total radiative forcing, global mean surface temperature, and sea level rise are shown as anomalies from the 2001-2010 average, while emissions and CO_2 concentration are absolute values. **Row two**) As Row one, but showing the difference between the 2020 CO_2 "pulse" simulations, in which a pulse of carbon emissions in year 2020 is added to the baseline carbon emissions for each RFF-SP draw, and the control simulations for each climate variable. The pulse size is identical across all RFF-SP draws and thus, there is no uncertainty in column one. **Row three**) As Row two, but for a pulse of Methane (CH_4). **Row four**) As Row two but for a pulse of Nitrous Oxide (N_2O). All GHG baseline and pulse emissions in column one are shown in the units in which they are entered into FaIR. See Table 1.

A key criterion for the climate module is the ability to probabilistically represent the uncertainty in the carbon-climate system in line with the latest scientific evidence. To satisfy this, we run FaIR with

a set of calibrated input parameters that were developed for use in the AR6 and determine the global mean temperature response to emissions (see (*19*) Box 7.1 and Chapter 7 Supplementary Material 7.SM.2 for additional details). These parameters are the result of constraining a 1 million-member ensemble of emissions-driven FaIR simulations over 1750-2019, as described in Ch. 7 of AR6 WG1 and its Supplementary Material (Section 7SM.2). The input parameters sample uncertainty in effective radiative forcing (ERF), the climate response (surface and deep ocean effective heat capacities, efficacy of ocean heat uptake, heat transfer coefficient between the surface and deep ocean layers, and climate feedback parameter) and the carbon cycle (airborne fraction of CO_2, and change in airborne fraction of CO_2). The constrained parameter set includes 2,237 members (*20*)[10] that satisfy criteria for matching the trend in historical global average temperature, the assessed historical ocean heat uptake, 2014 atmospheric CO_2 concentrations, and airborne fraction of CO_2 concentrations in transient CO_2 increase simulations. These parameters yield climate simulations that are consistent with the assessed ranges of equilibrium climate sensitivity (ECS) and transient climate response (TCR), and the ranges of GMST change for the AR6 emissions scenarios (see Ch 7 Cross-Chapter Box 7.1 of (*19*)).

A full representation of the emissions uncertainty combined with the climate uncertainty, even in a lightweight climate model such as FaIR, is infeasible as it requires over 22 million simulations (10,000 RFF-SPs x 2,237 climate parameters) for each pulse gas and pulse year. Instead, the 10,000 RFF-SPs were jointly sampled with the 2,237 climate parameters 10,000 times with replacement. The result is a set of 10,000 draws of an RFF-SP emissions pathway paired with one set of FaIR climate parameters. The final ensemble of RFF-SP-FaIR-climate-parameter draws yields 6,282 unique RFF-SPs, 2,208 unique climate parameters, and 9,997 unique pairs. The RFF-SP to FaIR input parameter pairings were selected to ensure consistency across socioeconomics and climate modules used within the EPA report. The climate response to the combined RFF-SP emissions and climate uncertainty is shown in Figure 2.

For the coastal sector, we also must represent GMSL with and without a pulse, as we do GMST, in order to compute marginal coastal damages conditional on GMSL, due to a pulse of GHG emissions. Because GMSL is not an output of the FaIR model, a process for deriving time series of GMSL from GMST time series is developed and involves using the Semi-Empirical Sea Level (SESL) model to calculate GMSLs from GMSTs with and without a pulse. These derived GMSLs are differenced to produce a pulse "delta", which is then added to probabilistic baseline GMSL trajectories modeled using the Framework for Assessing Changes to Sea-level (FACTS), used in the IPCC's AR6(*21*). We use a quantile mapping approach to align the pulse deltas with the baseline GMSL time series to produce GMSL trajectories with and without a pulse. Lastly, because the FACTS-based baselines are limited to the CMIP6 emissions pathways and do not include RFF-SP emissions, we approximate baseline GMSL time series for each RFF-SP-FaIR climate parameter draw using an emulation approach. Details of the development of the GMSL time series are described in Appendix C.5.

[10]The v1.0 parameter set was downloaded from https://doi.org/10.5281/zenodo.5513022.

These probabilistic simulations of global mean surface temperature and global mean sea level are used to derive probabilistic damage streams due to the baseline emissions and to a marginal pulse of emissions.

4 Damages Module

Here we first describe our approach to creating global "damage functions" that are reflective of the emissions, population, and economy represented in each of the RFF-SP simulations, and that relate changes in GMST (and GMSL for coastal damages) to changes in global damages[11]. This process involves estimating high resolution local dose response functions (Section 4.1.1) for each economic sector that we model[12], projecting those local dose response functions into the future to estimate local damages in the future (Section 4.1.2), and aggregating local damages to the globe and estimating global damage functions (Section 4.2), with sector-specific details provided in Appendix C. We then describe the application of the global damage functions to probabilistic FaIR GMST and GMSL trajectories to arrive at streams of damages representative of RFF-SP socioeconomics and emissions uncertainty and climate uncertainty (Section 4.3). Note that the location- and sector-specific outputs are consistent across DSCIM-EPA user options and pre-computed, due to the large compute footprint associated with producing these outputs.

4.1 Dose response function estimation and projection

4.1.1 Estimation

Our approach to estimating damages begins with collecting globally representative, high-resolution datasets of socioeconomic outcomes, such as death rates and electricity demand, matched to the high-resolution historical weather data described in section 3.1.1. We analyze these data using sophisticated econometric techniques, which account for the many geographic, institutional, and cultural differences between regions as well as trends over time, in order to estimate causal (rather than correlative) relationships between weather and our outcomes of interest. The result of this analysis is a location-specific "dose response" function: a description of the nonlinear effect of changes in temperature (and other weather variables for some sectors) on an outcome of interest. To capture the potential for adaptation and dynamic vulnerability, we include climate and socioeconomics in this estimation process, allowing the dose response function to vary with income levels and climatic adaptation.

The exact form of the dose response function varies across sectors but has the same purpose - estimating how climate variables like temperature affect some outcome (e.g. mortality risk, energy consumption), while accounting for adaptation based on access to resources (i.e. income) and the long-run climate. In general, a location-specific annual damage outcome takes the form:

[11] At the end of this Section, we also describe damage functions that include only direct damages within the territorial U.S.

[12] These are mortality, energy, labor, agriculture. We also model the coastal sector, but it relies on a process-based model and does not estimate dose response functions.

$$D_{scit} = f_{sc}(T_{it}\ ,\ LONGRUNCLIM_i, \log(GDPpc)_i) + q_{sc}(OTHERCLIM_{it}) + \alpha_{sci} + \gamma_{sct} + \epsilon_{scit} \quad (1)$$

where s indicates economic sector, c indicates category of damage outcome (e.g. age group for mortality, fuel category for energy) with c varying by sector, i denotes the spatial regions of analysis (e.g. county, state, country, which varies by sector), and t indicates the time period (e.g. day, year, which varies by sector). Thus, D_{scit} is the sector-specific, category-specific damage outcome in spatial unit i at time period t. D_{scit} is a function of the temperature vector that captures the nonlinear transformations of daily grid-cell temperature (T_{it}), the long-run climate variable ($LONGRUNCLIM_i$), and the natural logarithm of annual per capita GDP ($GDPpc_i$).[13] The long-run climate and annual per capita GDP together determine how sensitive the outcome in a given location is to daily weather variations. D_{scit} may also be a function of transformations of other climate variables like precipitation, noted generally here as $q_{sc_s}(OTHERCLIM_{it})$.[14]

Our econometric specifications for each sector and category include some form of location-specific and time period-specific intercepts (α_{sci} and γ_{sct}, respectively), referred to as "fixed effects".[15] Location fixed effects flexibly account for all permanent differences in the outcome between locations (for example, due to geography or history), while time period fixed effects flexibly account for trends in the outcome that are common across locations (for example, due to macroeconomic fluctuations or technological innovations). The use of fixed effects purges our estimates of confounding variation, enabling us to identify a plausibly causal effect of temperature variation on the outcome. Finally, ϵ_{scit} denotes the stochastic error term.

The parameters that describe the dose-response function are estimated with uncertainty, which must be accounted for when using them to project the impacts of future climate change (see below). We account for this statistical uncertainty by resampling parameter values from their joint probability distribution. For greater detail on the econometric estimation in the mortality, energy, labor, and agriculture sectors, see (*4*) Section IV, (*3*) Methods: Econometric estimation of energy–temperature responses, (*22*) Section 4, and (*23*) Methods section, respectively, with summaries provided in Appendix C.

4.1.2 Projections

Next, we apply this dose-response function to future projections of local temperatures and socioeconomics. While we use the RFF-SPs for SC-GHG calculations, their use in global climate models (GCMs) is infeasible, since the time required to compute climate changes at the resolution of the models necessitates using far fewer scenarios of emissions. The climate science community has centered their analyses of climate change in the GCMs on the RCP scenarios from CMIP5. These RCPs trace out possible emissions scenarios that range from cases with ambitious mitigation of CO_2 to ones in which emissions continue to grow for much of

[13] The exact parameterization of the long-run climate varies by sector.
[14] The exact parameterization of other climate variables varies by sector.
[15] The exact parameterization of the fixed effects varies by sector.

this century. In our estimates of climate damages, we use climate projection data from two RCPs (RCP4.5 and RCP8.5) from CMIP5, as discussed in Section 3.1.2, in order to fill out the probable space of future warming.

A similar logic leads us to calculate damages using a more limited set of socioeconomic projections than the RFF-SPs. The shared socioeconomic pathways (SSPs) database provides these projections across five separate scenarios for the economic future of the planet. The SSPs propose a set of plausible scenarios of socioeconomic development over the 21st century in the absence of climate impacts and policy for use by the Integrated Assessment Modeling (IAM) and Impacts, Adaptation, and Vulnerability (IAV) scientific communities (*8*). Projections of national incomes under the SSP scenarios are provided by the Organization for Economic Co-operation and Development (OECD) Env-Growth model (*24*) and the International Institute for Applied Systems Analysis (IIASA) GDP model (*25*). The estimates of climate damages in DSCIM incorporate the SSP2, SSP3, and SSP4 scenarios under each of these two models, in combination with the two emissions pathways described above.

For our projections we apply the dose-response functions to the CMIP5 projected weather data, for each GCM. We perform projections across the multiple drivers of uncertainty in future projections, consisting of: (1) different emissions scenarios (across RCPs), (2) different modeled changes in climate (across GCMs), (3) different socioeconomic scenarios (across SSPs), (4) different modeled country-level incomes (across economic models), and (5) different values of the statistical uncertainty describing the dose-response functions.

To isolate the impacts of climate change from changes in vulnerability driven by socioeconomics, we also apply the dose-response functions to a scenario in which climate remains in its historical state while economies continue to develop. The final impacts of climate change are the difference between the full projected outcomes, including all future changes, and the projected outcomes accounting only for socioeconomic changes. Formally, the impact of climate change ($Impact$) in impact region r[16], at year y for economic sector s and damage category c takes the form:

$$\begin{aligned} Impact_{scry,lpjd} = & \underbrace{f_{sc,d}(T_{ry,lp}\ ,\ LONGRUNCLIM_{ry,lp}, \log(GDPpc)_{ry,j})}_{\text{(A) dose-response function applied to climate-change scenario}} \\ & - \underbrace{f_{sc,d}(T_{ry_0}\ ,\ LONGRUNCLIM_{ry_0}, \log(GDPpc)_{ry,j})}_{\text{(B) dose-response function applied to historical climate scenario}}. \end{aligned} \tag{2}$$

To capture multiple drivers of uncertainty, projections are separately carried out under each GCM l, RCP p, SSP j[17], and resampled estimate d of dose-response function parameters. The impact described in Equation 2 represents the change in a given outcome due to a shift in the temperature distribution under climate

[16]There are 24,378 approximately county-sized impact regions globally, each of which is agglomerated from second administrative units based on maintaining approximately similar population across regions and approximately similar average climate within each region. Details can be found in (*4*) and (*3*)

[17]Note that a subscript for growth model has been omitted to simplify notation.

change, accounting for the evolution of the dose-response function as locations warm and incomes increase. This construct isolates the additional impact of climate change net of other factors (for example, income) that will change in the future. The two objects being differenced, (A) and (B), are identical in every way, except for the climate.[18] Thus, we evaluate (B) using future levels of income but use T and $LONGRUNCLIM$ values from a historical baseline y_0.[19] [20]

The resulting impacts are typically in physical units, such as changes in death rates and agricultural yields. To translate these into economic damages, we apply a monetary value per physical unit. For example, in the mortality sector, the value of a statistical life (VSL)[21] represents how much individuals are willing to pay to reduce mortality risk in their own life and has the units of dollars per death. By multiplying projected changes in death rates from climate change with population (in each age category), we estimate total changes in premature deaths, which we then multiply with the VSL and sum across age categories to estimate total economic losses in dollar terms (*26*).[22] The VSL is used for valuation of heat and cold-related deaths in the mortality sector and for flood-related deaths in the coastal sector (the coastal sector also includes valuation of abandoned property, inundated land, flood-related property damages, protective measure construction, relocation, and wetland loss). The translation of impacts from physical units to monetary damages is specific to each sector and is described in detail in Appendix C. We also estimate the costs of adaptation, based on the observed changes in vulnerability that are represented in the dose-response functions. The total economic losses combine direct losses from climate change (expressed in Equation 2) and indirect costs of adaptation to avoid further climate change losses.

This procedure provides us with total economic losses in each location, year, and sector under each GCM, RCP, and SSP, for multiple draws capturing uncertainty in dose-response function parameter estimates. One way to handle such uncertainty is to simply calculate a mean over these multiple draws for each sector, before combining all sectors and aggregating to the globe. However, this fails to account for the fact that individuals are risk-averse and are willing to pay a risk premium to avoid potentially severe damages. For DSCIM-EPA results provided here, we calculate a value from the multiple draws that incorporates this risk premium by computing a certainty equivalent (CE) over the draws, referred to as the "risk averse" result (in contrast to the "risk neutral" result). The calculation is performed using a constant relative risk aversion (CRRA) utility function for various values of the elasticity of marginal utility of consumption, (denoted η)[23] as follows (see Appendix A for additional details)[24]. Relative to historical climatology (h), for each sector s, SSP j,

[18] All fixed effects and other controls included in Equation 1 cancel out and are therefore omitted.

[19] Note that the agriculture sector projects precipitation variables in addition to temperature, and they are also from the historical baseline.

[20] We define the baseline period y_0 as having the climatology of 1981-2005.

[21] We use the U.S. EPA's VSL for 2020 amounting to $9,926,524.56 (2019$). Additional details are in Appendix section C.1

[22] It should be noted that the VSL does not represent the value of an individual life. Rather it represents willingness-to-pay for a collective risk reduction of one "statistical life". For instance, if, on average, each individual is willing to pay $100 per year to reduce his/her probability of dying by 0.00001, then collectively a group of 100,000 people would be willing-to-pay $10 million per year to avoid the loss of one "statistical life".

[23] Eta values are $\eta = [1.016010255, 1.244459066, 1.421158116]$.

[24] To execute this calculation, we set a subsistence value for consumption equal to the minimum baseline income projected across all year, region, SSP combinations, which is equal to $39.39. For each region-year-SSP, we constrain the maximum

GCM l, RCP p and in each impact region r and year y, we compute damages per capita accounting for the risk premium as:

$$\begin{aligned} \text{Damages Per Capita}_{srjlpy} &= CE^{noCC}_{srjlhy} - CE^{CC}_{srjlpy} \\ \text{where } CE^{CC}_{srjlpy} &= \left(\left(\frac{1}{K} \sum_{d \in K} \frac{C^{1-\eta}_{srjdlpy}}{1-\eta} \right) * (1-\eta) \right)^{\frac{1}{1-\eta}} \\ \text{and } C_{srjdlpy} &= \text{GDPpc}_{rjy} - \text{Damages}_{srjdlpy} \end{aligned} \tag{3}$$

CE^{CC} represents the CE of consumption over dose response function uncertainty draws under climate change and is a function of η and local per capita consumption, C, in each of the draws, which we define as local GDPpc less damages in each draw. We similarly calculate the CE of consumption under a no-climate-change counterfactual scenario (CE^{noCC}), where uncertainty in local consumption exists due to variability in the local climate around its historical mean, and subtract it from the CE^{CC} to obtain the change in CE damages due to changes in climate[25]. We thus obtain a single measure that captures total economic losses (including the risk premium) in each location and year, within each GCM, RCP, and SSP combination and for each sector and η value.[26].

Note that our treatment of coastal damages from sea level rise uses a different modeling framework, due largely to the fact that historical sea level rise has been relatively minimal in most locations. This leaves little opportunity for robust empirical estimation of an economic response function that would be globally representative and applicable to future sea level rise. Instead, we employ a parameterized optimization model (pyCIAM, (*27*)) that calculates adaptation strategies and projects resulting future damages for 9,096 coastal segments using a least-cost optimization framework. Damages represented in this framework include (a) the cost of permanent inundation of immobile capital or land; extreme sea level-related (b) damages to capital and (c) mortality; (d) expenditures on protection (i.e. infrastructure construction); (e) relocation costs; and (f) wetland loss. Because of the use of this process-based approach, no empirical estimation step using historical outcomes is used within the coastal sector, and the projections for the coastal sector stem from a more process-based methodology.

damage draw such that consumption does not fall below the subsistence level.

[25]If we ignore this baseline uncertainty, we would overstate the risk premium by conflating weather variation with climate uncertainty. We therefore treat consumption uncertainty due to variability in the historical baseline climate in a similar manner as we treat uncertain damages due to climate change. Specifically, we calculate local no-climate-change consumption for each impact region in each Monte Carlo draw as GDP per capita minus climate "damages" due to historical climate variability (i.e., $C_{srjdlhy} = \text{GDPpc}_{rjy} - \text{"Damages"}_{srjdlhy}$, where the subscript h denotes the historical climatology instead of climate change under RCP p. We then take the certainty equivalent of consumption across these draws (i.e., $CE^{noCC}_{srjlhy} = \left(\left(\frac{1}{K} \sum_{d \in K} \frac{C^{1-\eta}_{srjdlhy}}{1-\eta} \right) * (1-\eta) \right)^{\frac{1}{1-\eta}}$).

[26]Note that accounting for the risk premium across climate uncertainty is handled by stochastic Ramsey discounting on the damages derived from probabilistic outputs from the FaIR reduce complexity climate model after global damage functions have been estimated. This is described in Section 5.1

4.2 Damage function estimation

The valued losses including the risk premium described in the previous section are used to estimate a global "risk averse damage function" for each sector and for the combined sectors. The damage function describes the globally aggregated economic losses that result from a given change in the global average climate. The "risk averse" damage function is fit to globally aggregated impact region level damages where a CE across dose response function draws (also referred to as Monte Carlo draws) has been taken in each impact region, collapsing the damages in each impact region as shown in Equation 3 before summation to the globe for each GCM × RCP × SSP combination. In contrast, a "risk neutral" damage function would be fit to globally aggregated impact region level damages where a *mean* across dose response function draws has been taken.

To construct such a risk averse damage function, we first index projected global economic losses in each year from 2020-2099, under each GCM × RCP pairing, to the change in GMST (ΔGMST) projected in the five-year window centered around that year under that pairing.[27] For each sector s[28], SSP j, and year y[29], we then estimate a damage function that is quadratic in ΔGMST, fit to points from 33 GCMs (l) across the two RCP emissions scenarios (p)[30]. This takes the form:

$$Damages_{slpyj} = \beta_1^{syj} \Delta GMST_{ylp} + \beta_2^{syj} \Delta GMST_{ylp}^2 + \epsilon_{slpyj} \tag{4}$$

where ϵ_{slpyj} denotes the stochastic error term. The coefficients[31] β_1^{syj} and β_2^{syj} are estimated by ordinary least squares. For all sectors except coastal, damage functions of the same functional form are estimated on ΔGMST variables. However, because coastal damages are a function of the change in GMSL (ΔGMSL) rather than ΔGMST, a damage function of the same form is estimated on ΔGMSL and ΔGMSL^2, where the GMSL values are as described in Appendix C.5. The damage function representing the combined 5-sector damages is a concatenation of the estimated damage function on (agriculture + mortality + energy + labor) with the damage function estimated on coastal, such that the damage function has four coefficients, two of which act on ΔGMST variables and two of which act on ΔGMSL variables. Thus damages under a given ΔGMST and ΔGMSL pair are obtained by summing damages from coastal (conditional on ΔGMSL) and damages for the combined 4 sectors of agriculture, mortality, energy, and labor (conditional on ΔGMST).

This results in a set of damage functions that spans the space of the GMSTs and GMSLs and global damages that are based on the three SSP socioeconomic pathways[32] and two RCP emissions pathways. To

[27] ΔGMST is relative to the 2001-2010 average.

[28] Sectors include agriculture, coastal, energy, labor, mortality, and their combination. The five-sector combination consists of summing damages across sectors at the impact region level for each GCM and dose response function draw, before computing either the mean (risk neutral) or the CE (risk averse) in that impact region, and aggregating to the globe.

[29] The damage function also depends on η but we leave out a subscript for parsimony.

[30] In actuality, the damage functions are fit to points inclusive of a 5-year centered window around y.

[31] Damage function coefficients are installed during DSCIM-EPA installation and setup, after which they reside inside of /PATH/TO/dscim-epa/input/damage$_f unctions/.DSCIM - EPAisavailableathttps$: $//github.com/ClimateImpactLab/dscim - epa$.

[32] Note the damage functions are also spanning two growth models, IIASA and OECD. In total there are 6 risk averse damage

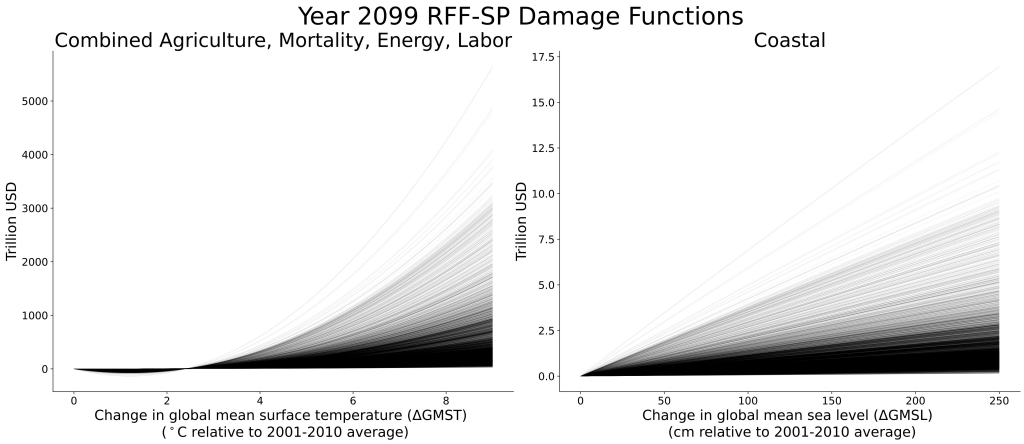

Figure 3: RFF-SP Risk Averse Global Damage Functions: Risk averse global damage functions for all 10,000 RFF-SP draws (this maps to 6,282 unique damage functions due to the sampling with replacement described in Section 3.2) are shown for the combined sectors conditional on ΔGMST (agriculture + mortality + energy + labor; left panel) and for coastal, conditional on ΔGMSL (right panel) for the year 2099. The draw-specific combination of these two sets of damage functions makes up the combined five-sector damage functions used in the combined SC-GHG calculation.

construct damage functions that are based on the RFF-SPs (*10*), which are used to calculate the SC-GHGs, we use these SSP-based damage functions to emulate global damage functions for an arbitrary draw of an RFF-SP. The same approach is used for emulating damage functions that are conditional on ΔGMST and those conditional on ΔGMSL. The emulation procedure is as follows:

1. We denominate our estimated annual SSP-based damage functions as a share of annual global GDP from the SSP.

2. We calculate a set of weights, constrained to sum to unity, that, when used to take a weighted average of global GDP across SSP-growth models, most closely recovers the global GDP in the RFF-SP simulation run that we wish to emulate.

3. We apply these weights to take a weighted average of the redenominated damage functions from Step 1.

4. Finally, we convert this new, emulated RFF-SP-specific damage function into an economy-wide measure of total dollar damages by multiplying by RFF-SP-specific global GDP. This results in a damage function denominated in total dollar damages.

This emulation procedure provides us with damage functions for each of the RFF-SP draws k which are then used in SC-GHG calculations. Full details about the emulator can be found in Appendix B. Figure 3 shows the combined-sector GMST-based global risk-averse damage functions on the left and global coastal

functions – 3 SSPs x 2 growth models – each of which is fit on GMST points from 2 RCPs (RCP4.5 and RCP8.5 from CMIP5). Because GMSL is not an output of the GCM data we use, a different method to compute GMSL points is developed and described in Appendix C.5.

risk-averse damage functions on the right for all RFF-SP draws. These damage functions are independent of pulse gas, pulse size, pulse year, FaIR climate draw[33], Weitzman parameter (see Section 5.2), discounting type, and pure rate of time preference ρ.

Lastly, because the GCM simulations and the SSPs end in 2099 but SC-GHG calculations depend on damages out to 2300, an extrapolation of these time-varying damage functions must be performed. To calculate the damage function in years $y > 2099$, we extrapolate the 2099 damage function as follows: Let $\beta_1^{s,y,k}$ and $\beta_2^{s,y,k}$ denote the coefficients of the sector s, year y emulated damage function under RFF-SP simulation run k. To obtain coefficients for years $y > 2099$, the 2099 damage function coefficients are multiplied by the ratio of RFF-SP simulation k global GDP in year y to its 2099 global GDP, i.e.:

$$\beta_m^{s,y,k} = \beta_m^{s,2099,k} \times \frac{\text{RFFGDP}_{ky}}{\text{RFFGDP}_{k,2099}} \tag{5}$$

for $m = \{1, 2\}$.

A set of SC-GHGs limited to the direct damages occurring within the territorial United States is also available. These are computed using the same method that has just been described above, except only impact regions within the United States border are included in the aggregation step. This is only a partial accounting of the cost of climate change to US citizens and residents because it excludes international transmission mechanisms, like trade, cross-border investment and migration, damage to the assets of U.S. citizens and residents outside the United States, or consideration of how GHG emission reduction activity within the United States impacts emissions in other countries.

4.3 Calculation of probabilistic damage streams using FaIR climate outputs

Once a damage function is estimated, it can be applied to the probabilistic ΔGMST trajectories produced by FaIR and ΔGMSL trajectories emulated with SESL and FACTS (as described in Section 3.2). The procedure to produce damage streams is as follows:

For each sector s, year y, and for each RFF-SP draw k (RFF-SP paired with a climate parameter set)[34]:

1. Calculate damages due to climate change using the emulated RFF-SP specific damage function coefficients. We refer to these damages as Damages^{nopulse}, since they are computed using Δ GMST from the FaIR model run with RFF-SP k baseline emissions, without an additional pulse of greenhouse gas

[33]The damage functions are independent of FaIR climate draw, except for the fact that the climate parameter is paired with an RFF-SP draw

[34]These calculations also vary by eta value (η) because the damage function coefficients vary by η. This is due to the η in the CRRA utility function used within each impact region to calculate the damages including the risk premium to avoid severe damages (See Equation 3), before aggregation to the globe for damage function estimation. We leave out a subscript for eta for parsimony.

emissions[35]:

$$\text{Damages}_{syk}^{nopulse} = \beta_1^{syk} \Delta\text{GMST}_{yk}^{nopulse} + \beta_2^{syk} (\Delta\text{GMST}_{yk}^{nopulse})^2. \tag{6}$$

2. Calculate global consumption under climate change by subtracting these baseline damages from RFF-SP GDP. In DSCIM-EPA this object is referred to as "global consumption no pulse".

$$\text{GlobalC}_{syk}^{nopulse} = \text{RFFGDP}_{yk} - \text{Damages}_{syk}^{nopulse} \tag{7}$$

Then, for each pulse year u and greenhouse gas o:

3. Calculate damages due to climate change under the RFF-SP emissions plus a "pulse" of emissions in the pulse year as in Equation 6[36]. The pulse of emissions in year u causes damages in all years $y >= u$.

$$\text{Damages}_{sykuo}^{pulse} = \beta_1^{syk} \Delta\text{GMST}_{ykuo}^{pulse} + \beta_2^{syk} (\Delta\text{GMST}_{ykuo}^{pulse})^2. \tag{8}$$

4. Calculate global consumption under climate change *with the pulse* by subtracting these pulse damages from RFF-SP GDP. In DSCIM-EPA this object is referred to as "global consumption pulse".

$$\text{GlobalC}_{sykuo}^{pulse} = \text{RFFGDP}_{yk} - \text{Damages}_{sykuo}^{pulse} \tag{9}$$

5. Calculate marginal damages by subtracting damages without the pulse from damages with a pulse.

$$\text{MarginalDamages}_{skyuo} = \text{Damages}_{sykuo}^{pulse} - \text{Damages}_{syk}^{nopulse} \tag{10}$$

This results in a set of 10,000 probabilistic time series of marginal damages due to a pulse of GHG emissions, as well as global consumption under climate change with and without an extra pulse of emissions, for each sector, GHG, and pulse year. Marginal damages can then be discounted as described in Section 5 using discount factors calculated from the global consumption, $\text{GlobalC}^{nopulse}$, paths. The final SC-GHG calculation is described in detail in Section 6 after a summary of steps leading up to the final calculation.

[35] When computing the coastal partial SC-GHG and the coastal component of the combined 5-sector SC-GHG, the same approach is used except $\Delta\text{GMSL}_{yk}^{nopulse}$ is used in place of the $\Delta\text{GMST}_{yk}^{nopulse}$ variables.

[36] When computing the coastal partial SC-GHG and the coastal component of the combined 5-sector SC-GHG, the same approach is used except $\Delta\text{GMSL}_{ykuo}^{pulse}$ is used in place of the $\Delta\text{GMST}_{ykuo}^{pulse}$ variables.

5 Discounting Module & Valuation

5.1 Discounting Procedure

In the DSCIM-EPA SC-GHG calculation, we implement continuous time Ramsey discounting to discount damages back to the pulse year u.[37] Specifically, we use the Ramsey discount rate consistent with the rate of consumption growth in each RFF-SP draw k, *inclusive* of climate damages. The stochastic discount factor for damages in RFF-SP draw k and in year $y > u$ is set as follows:

$$SDF_{ky} = \prod_{\tau=u+1}^{y} e^{-(\rho+\eta\tilde{g}^{c}_{k\tau})} \tag{11}$$

where the rate of consumption growth inclusive of climate damages, $\tilde{g}^{c}_{k\tau}$, is given by $ln\left(\frac{c_{k\tau}}{c_{k,\tau-1}}\right)$. In each year τ, ${c_{k\tau}}$[38] is given by Equation 9— baseline global GDP in the given RFF-SP draw minus the damages associated with the GMST anomaly from the RFF-SP FaIR climate parameter draw[39]. The parameter ρ measures the pure rate of time preference, while η is the elasticity of marginal utility of consumption.

Note that since marginal damages in each draw are discounted at the stochastic discount rate consistent with that draw,[40] this discounting approach adjusts for all dimensions of the intertemporal tradeoff: the rate of baseline economic growth, the severity of climate change, and the correlation between payoffs from climate change mitigation and the future state of the world. Each dollar of future losses is thus valued according to the Ramsey formula's comparison of future and present marginal utility appropriate to that particular draw.

We implement this discounting approach using three alternative sets of $\{\eta, \rho\}$ combinations obtained from (*10*) to match near-term rates of 1.5 percent, 2.0 percent, and 2.5 percent[41].

Lastly, the expected SC-GHG is computed by taking the net present value of discounted marginal damages in each RFF-SP draw, applying an adjustment to account for consumption uncertainty before the pulse year, and then averaging the adjusted net present values across RFF-SP draws. This process is described in detail in Step 8. of the next section, Section 6.

5.2 The Weitzman parameter

To confront issues related to climate uncertainty where damages can exceed global GDP causing mathematically undefined stochastic discount factors, we introduce an additional parameter inspired by the work of

[37] In Section 6.1 Step 8, we describe an additional procedure to discount damages back to the present, accounting for uncertainty between the present and the pulse year u.

[38] For compactness, we use the variable symbol "c_{ky}" instead of "$GlobalC^{nopulse}$", as in the previous section, to represent global consumption no pulse.

[39] As described in 3.2, the RFF-SPs and FaIR climate parameters are sampled jointly such that an RFF-SP is paired 1:1 with a set of FaIR climate parameters.

[40] Specifically, marginal damages in a given year under a given RFF-SP draw are discounted by multiplying by the SDF for that year and draw.

[41] These η and ρ combinations are η, ρ = [1.016010255, 9.149608e-05], [1.244459066, 0.00197263997], [1.421158116, 0.00461878399] matching 1.5%, 2.0%, and 2.5% near-term rates, respectively.

Martin Weitzman (e.g. (*28*)) that caps global damages due to climate change. We define the "Weitzman parameter", ω, to be a scalar fraction from 0-1 that is used to calculate the "Weitzman threshold". The Weitzman threshold, $\underline{C}_{ky}$, is the value of the share of contemporaneous GDP in each year and RFF-SP that serves to top-code marginal utility and constrain global damages such that the Ramsey discounting calculation is always defined.

Formally, for unadjusted consumption c_{ky} (baseline global GDP, RFFGDP_{ky}, minus the damage draw) and Weitzman threshold $\underline{C}_{ky}$, we define an adjusted consumption value, $\hat{c}_{ky}$, as follows:

$$\hat{c}_{ky} = \begin{cases} c_{ky} \; if \; c_{ky} \geq \underline{C}_{ky} \\ U^{-1}\Big(U(\underline{C}_{ky}) - U'(\underline{C}_{ky}) \times (\underline{C}_{ky} - c_{ky})\Big) \; if \; c_{ky} < \underline{C}_{ky} \end{cases} \tag{12}$$

where

$$\underline{C}_{ky} = \omega * \text{RFFGDP}_{ky} \tag{13}$$

Implemented with a CRRA utility function with utility curvature parameter η, $\hat{c}_{ky}$ becomes:

$$\hat{c}_{ky} = \begin{cases} c_{ky} \; if \; c_{ky} \geq \underline{C}_{ky} \\ \Big[\underline{C}^{1-\eta} - (1-\eta) * (\underline{C}_{ky}^{-\eta})(\underline{C}_{ky} - c_{ky})\Big]^{\frac{1}{1-\eta}} \; if \; c_{ky} < \underline{C}_{ky} \end{cases} \tag{14}$$

The intuition of this equation is that the Weitzman parameter top codes the marginal utility of consumption at the value of $\underline{C}$, allowing each dollar of losses below $\underline{C}$ to have the same marginal utility as that at the level of $\underline{C}$. Total utility is then calculated including the utility costs below the bottom coded value, and then converted back into an equivalent consumption value, $\hat{c}_{ky}$, by inverting the utility function. Then $\hat{c}_{ky}$ enters directly into the Ramsey discounting calculation in a standard way, replacing c_{ky}. In this way, the choice of the Weitzman parameter, ω and by proxy the Weitzman threshold, $\underline{C}_{ky}$, governs how quickly global consumption declines under bad climate outcomes.

6 Putting it all together: the SC-GHG calculation

The previous sections describe the DSCIM-EPA implementation of each of the SC-GHG component modules following recommendations by the NASEM(*1*). Next we summarize how DSCIM-EPA uses these modules in a step-by-step process for calculating sector-specific and combined SC-GHGs for a range of pulse years.

6.1 Step by step process to SC-GHGs

1. **Local Climate Damage Projections:** This step is described in detail in Section 4.1.2 and Appendix C.

We generate Monte Carlo draws of local climate damages across dose response function uncertainty for the five sectors – agriculture, coastal, energy, labor, and mortality – using projections for 24,378 approximately U.S. county-sized "impact regions" spanning the world in each future year. These damage projections are pre-computed for CMIP5 RCP4.5 and RCP8.5 emissions pathways paired with SSP2, 3, and 4 using GDP growth from IIASA and from OECD growth models, resulting in 12 projection simulations (each with Monte Carlo uncertainty) for each of 33 GCMs, for the combined five sectors, and for each of the five individual sectors.

This step varies by the following DSCIM-EPA user options: sector.

2. **Calculation of the Local Welfare Costs of Climate Change:** This step is described in detail in Section 4.1.2.

   Next, for each of the 12 outputs in Step 1, we calculate the local welfare loss from the range of projected climate damages in each impact region in each GCM, for each sector and for the total damages across the five sectors[42]. DSCIM-EPA presents SC-GHGs using a calculation that incorporates the local risk premium to avoid potentially severe harm arising from econometric uncertainty.

   This calculation proceeds as follows. For each damage realization, we calculate local consumption for each impact region in each Monte Carlo draw as GDP per capita minus climate damages. We then take the CE of consumption across Monte Carlo draws to calculate expected welfare with climate change, accounting for risk aversion to the uncertainty in the damage estimates.[43][44] We similarly calculate expected welfare under a no-climate-change counterfactual scenario, where uncertainty in local consumption exists due to variability in the local climate around its historical mean.[45] The damage caused by climate change, including the risk premium, is then calculated as expected welfare under a no-climate-change counterfactual scenario minus expected welfare with climate change.

   This step varies by the following DSCIM-EPA user options: η, sector

3. **Climate Damage Aggregation:** This step is described in Section 4.2.

   Once we calculate local damages inclusive of the risk premium over damage uncertainty in Step 2, we aggregate local climate damages to the global level[46] for each GCM, RCP, SSP-growth model, and future year to estimate a damage function for each future year and SSP-growth model scenario.

[42] Damages are totalled by summing the sectors for each Monte Carlo draw.

[43] We use the constant relative risk aversion (CRRA) utility for this calculation with three different values of the elasticity of marginal utility of consumption ($\eta = [1.016010255, 1.244459066, 1.421158116]$).

[44] To execute this calculation, we set a subsistence value for local consumption equal to the minimum baseline income projected across all year, region, SSP combinations. We constrain the maximum damage draw such that consumption does not fall below the subsistence level.

[45] If we ignore this baseline uncertainty, we would overstate the risk premium. We therefore treat consumption uncertainty due to variability in the historical baseline climate in a similar manner as we treat uncertain damages due to climate change. Specifically, we calculate local no-climate-change consumption for each impact region in each Monte Carlo draw as GDP per capita minus climate "damages" due to historical climate variability. Taking the certainty equivalent of consumption across these draws yields expected welfare in the no-climate-change counterfactual scenario.

[46] Or we aggregate local climate damages to the U.S. level in the case of SC-GHGs that include only the direct damages within the territorial U.S.

This step varies by the following DSCIM-EPA user options: η, "global" versus "territorial U.S.", sector

4. **Damage Function Estimation in Each Future Year:** This step is described in Section 4.2.

   The aggregated damages from Step 3 span the range of GMST over which to estimate sector damage functions (except coastal), as described in Section 4 and Appendix C. Probabilistic sea level rise projections from LocalizeSL span the range of GMSL over which to estimate the coastal damage function, as described in Appendix C.5. Damage functions are estimated on globally (or U.S.) aggregated points from all GCMs under CMIP5 RCP4.5 and RCP8.5 emissions such that a greater range of GMST and GMSL are supported. These damage functions are quadratic in GMST and GMSL and have zero-intercept[47]. As described in 4.2 and Appendix B, these six SSP-based damage functions are then used to emulate a damage function for each of the 10,000 RFF-SP draws to emulate what aggregated damages may have looked like if a fully resolved spatial projection of each RFF-SP emissions and socioeconomics pathway could be executed. The result is a set of 10,000 RFF-SP-based damage functions[48].

   This step varies by the following DSCIM-EPA user options: η, "global" versus "territorial U.S.", sector. For efficiency and ease of replication for the EPA report, DSCIM-EPA begins computations from pre-computed RFF-SP damage function coefficients.

5. **FaIR Model Projections of Changes in GMST and GMSL:** This step is described in detail in Section 3.2.

   We use the FaIR reduced-complexity climate model to simulate GMST trajectories based on the 10,000 draws of RFF-SP and climate parameter pairings representing the probabilistic distribution of the change in GMST under emissions and climate uncertainty, with and without the marginal pulse of GHG emissions. We use a Semi-Empirical Sea Level model to obtain probabilistic GMSL estimates consistent with each GMST Monte Carlo draw, as described in Section C.5. One set of 10,000 control (or baseline) simulations are produced, and 21 sets of 10,000 pulse simulations are produced – one for each of 3 gases (CO_2, CH_4, and N_2O) $\times$ 7 pulse years (2020, 2030, 2040, 2050, 2060, 2070, and 2080) for both GMST and GMSL variables. These FaIR simulations are pre-computed and as such pulse size is predetermined (see Table 1) and not modifiable, and pulse year and gas can only be selected from the above lists.[49]

[47] When combining damage functions from coastal and non-coastal sectors, we estimate 1-dimensional damage functions (i.e. vs. GMST and GMSL, respectively) separately and then combine the outputs. While this approach will not capture the risk premium associated with the simultaneous experience of coastal and non-coastal losses, it avoids large coefficient biases that can be introduced when estimating a 2-dimensional damage function (i.e. vs. GMST and GMSL, simultaneously) that is constrained to pass through the origin.

[48] There are 6,282 unique RFF-SPs in the 10,000 RFF-SP draws as described in 3.2, however we produce a set of damage function coefficients for all 10,000 RFF-SP draws even though some are duplicate for ease of computation. Damage functions do not vary by FaIR climate parameter.

[49] One could in principle generate new GMST and GMSL paths in response to RFF-SP emissions baselines – using FaIR or other simple climate and sea level models – that represent different GHGs, pulse years, or pulse sizes. These could then be set as DSCIM-EPA inputs, provided the file and data structure were identical to existing data inputs.

This step varies by the following DSCIM-EPA user options: GHG, pulse year

6. **Calculation of Undiscounted Marginal Damages Associated with a Pulse of Emissions:** This step is described in Section 4.3.

   We use the 10,000 RFF-SP FaIR climate paramter draws for each GHG and pulse year from Step 5 to calculate the damage caused by the climate change baseline (emissions from the RFF-SP draw), and by a pulse of GHG emissions added to the baseline in the pulse year. Damage functions estimated in Step 4 are applied to the GMST temperature outputs (or GMSL in the case of the coastal sector and combined five sectors) from Step 5 to obtain damages in each future year with and without a pulse of emissions. Marginal damages are equal to damages with a pulse of emissions minus the damages without a pulse. Marginal damages are produced for each of the 10,000 RFF-SP draws, for each η.

   This step varies by the following DSCIM-EPA user options: η, "global" versus "territorial U.S.", sector, GHG, pulse year

7. **Discount the Stream of Future Damages:** This step is described in detail in Section 5.1.

   We discount, using stochastic Ramsey discounting, each of the streams of marginal damages caused by the pulse of emissions from Step 6 by taking into account future GDP *after* removing climate damages. Discount factors are a function of "global consumption no pulse" after top-coding the marginal utility based on the Weitzman parameter.

   This step varies by the following DSCIM-EPA user options: η, the pure rate of time preference ρ[50], "global" versus "territorial U.S.", sector, GHG, pulse year [51]

8. **Calculate the Cost Per Ton of GHG**

   The discounted streams of marginal damages for each RFF-SP draw from Step 7 represent the distribution of present values in each year from the pulse year to 2300. To compute the SC-GHG for each of the 10,000 RFF-SP draws k, we calculate the net present value of marginal damages in the draw (i.e., by summing present values from pulse year u to 2300) and divide this value by the number of tons of GHG in the pulse. This results in a distribution over k of the social cost per ton of greenhouse gas emissions for each sector s, GHG o, and pulse year u.

$$\text{PDVDamages}_{skuo} = \sum_{y=u}^{2300} \text{SDF}_{sky} * \text{MarginalDamages}_{skyuo} \tag{15}$$

[50] η and ρ can only be selected in pre-determined pairs that represent near-term discount rates of 1.5%, 2.0%, 2.5% from (*10*)

[51] Note that for the SC-GHG calculations that include only direct damages occurring within the territorial U.S., the stochastic discount factor is still computed using global GDP less *global* damages, since U.S. damages would be occurring in a world with global damages. In this way this SC-GHG is discounted using the same rate and can be directly compared to the global SC-GHG.

$$\text{SC-GHG}_{skuo} = \frac{\text{PDVDamages}_{skuo}}{\text{Tons}^{pulse}} \tag{16}$$

These SC-GHGs do not account for the uncertainty in growth occurring before the pulse year when marginal damages are zero. To account for this, an adjustment factor is computed that adjusts SC-GHG$_{skuo}$, such that for pulse year u (adopting the notation for global consumption no pulse, c_{sky} from Section 5):

$$\text{AdjustmentFactor}_{sk,y=u} = \left(\frac{c_{sk,y=u}}{\text{RFFPop}_{k,y=u}}\right)^{-\eta} * \frac{1}{E[c_{sk,y=u}]} \tag{17}$$

$$\text{CESC-GHG}_{skuo} = \text{AdjustmentFactor}_{sku} * \text{SC-GHG}_{skuo} \tag{18}$$

In this way, the CESC-GHG, or "certainty equivalent" SC-GHG, is the social cost of greenhouse gas that has been adjusted to include the risk premium for consumption uncertainty occurring before the pulse year. See the EPA's Report on the Social Cost of Greenhouse Gases for a detailed explanation of the motivation and derivation of this approach.

The final expected SC-GHG, ExpectedSC-GHG, is the mean over all 10,000 CESC-GHGs[52] and converted from 2019$ to 2020$[53]:

$$\text{ExpectedSC-GHG}_{suo} = \frac{1}{10000}\sum_{k=1}^{10000} \text{CESC-GHG}_{skuo} \tag{19}$$

This step varies by the following DSCIM-EPA user options: η, the pure rate of time preference ρ, "global" versus "territorial U.S.", sector, GHG, pulse year.

6.2 DSCIM-EPA user options and defaults

[52]This procedure adjusts for all dimensions of the intertemporal tradeoff. Taking the mean over draw-specific Ramsey discounted SC-GHGs is in fact equivalent to calculating the difference between certainty equivalents (over RFF-SP draws) of global consumption without a pulse and with a pulse, and then applying annual stochastic discount factors that reflect the growth rate of the (no pulse) global consumption certainty equivalent.

[53]We report SC-GHGs in 2020$ using the 2019 to 2020 price level deflator 113.648/112.294, obtained from https://apps.bea.gov/iTable/iTable.cfm?reqid=19step=3isuri=1select$_{a}ll_{y}ears$ = 0$nipa_{t}able_{i}ist$ = 13$series$ = $a first_{y}ear$ = 2005$last_{y}ear$ = 2020$scale$ = −99$categories$ = $surveythetable$ =

User Option	Options	Default	Notes
Pulse year	2020, 2030, 2040, 2050 2060, 2070, 2080	All pulse years	
Sector	combined (CAMEL) coastal agriculture mortality energy labor	combined	5-sector combined SC-GHG is internally referred to as CAMEL
η, ρ	[1.016010255, 9.149608e-05] [1.244459066, 0.00197263997] [1.421158116, 0.00461878399]	all rates	1.5% near-term rate 2.0% near-term rate 2.5% near-term rate
Domain	Global, Territorial U.S.	Global	Scope of damages included in the SC-GHGs, global or direct damages within territorial U.S.
Settings	**Value**		**Notes**
GHG	CO_2 , CH_4, N_2O	All GHGs	
pulse_size	1 GtC 40 MtCH4 1 MtN2		CO_2 pulse size CH_4 pulse size N_2O pulse size
weitzman_parameter	0.5		50% of RFFGDP
fair_aggregation	“uncollapsed"		draw-specific discounting produces distribution of SC-GHGs

Table 2: This table describes the DSCIM-EPA user options (top table), and settings for other options that are not modifiable (bottom table).

A Appendix: Accounting for risk aversion

A.1 The certainty equivalent

Figure 4 illustrates the concept of risk aversion via a heuristic example in which uncertain consumption under climate change takes a value of either C^{CC_1} or C^{CC_2} with equal probability. Mean damages from climate change (i.e., "risk-neutral damages") are equal to the difference between the no climate change level of consumption (C^{noCC}) and the average level of consumption under climate change ($\overline{C}^{CC}$). The certainty equivalent level of consumption under climate change (CE^{CC}) is defined as the level of consumption that provides utility equal to the expected utility of consumption across the 2 probabilistic possible states of the world. The difference between the no climate change level of consumption and the certainty equivalent level of consumption under climate change represents the "risk-averse damages" from climate change, reflecting the additional amount that risk-averse individuals are willing to pay over and above the average loss from climate change in order to avoid the chance of especially bad outcomes.

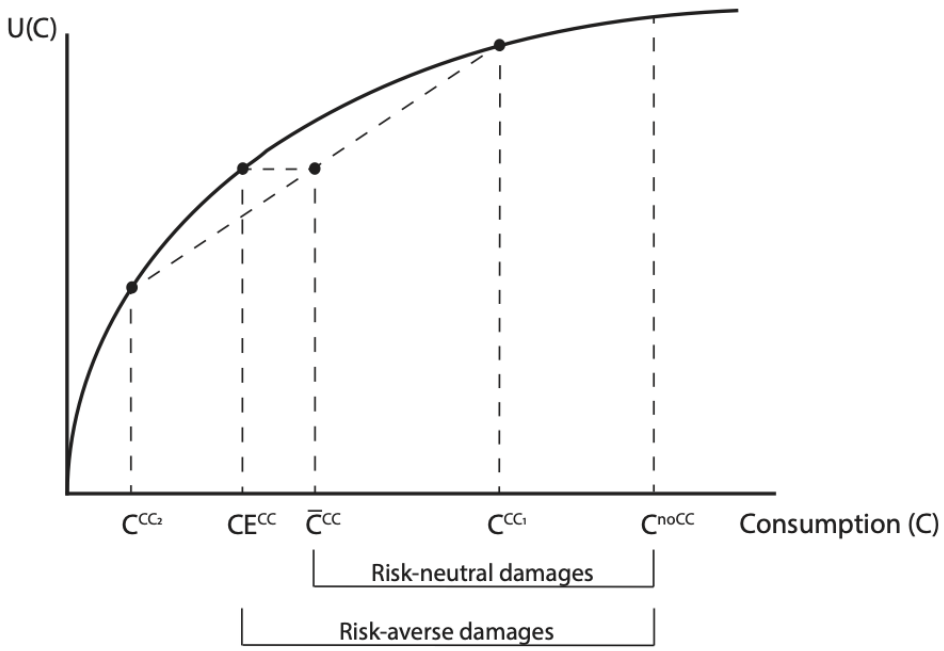

Figure 4: CE cartoon Here is a schematic that describes the CE calculation.

A.2 Illustration of risk averse damage function

As described in the main text (Section 4.1.2), dose response function uncertainty is sampled within each impact region and GCM resulting in uncertain damages depending on how sensitive the damage is to local

weather. In order to account for the risk-averse agent who is willing to pay to avoid the possibility of severe harm, a CE across damage uncertainty within impact region and GCM is calculated. Alternatively, to represent an agent that is risk neutral and unwilling to pay for such certainty, a mean across damage uncertainty within impact region and GCM is taken.

Once damages representing dose response function uncertainty are calculated for each impact region, they are aggregated across all regions of the world to the global level separately for each global climate model in each future year. Each climate model projects a different change in global mean surface temperature relative to 2001-2010 ($\Delta GMST$) in each emissions scenario, allowing us to estimate how global damages in a given year vary with $\Delta GMST$ in that year. The type of global damage function is determined by whether the local damage uncertainty was collapsed with a CE (risk averse) or a mean (risk neutral). Figure 5 illustrates such damage functions for the end-of-century.

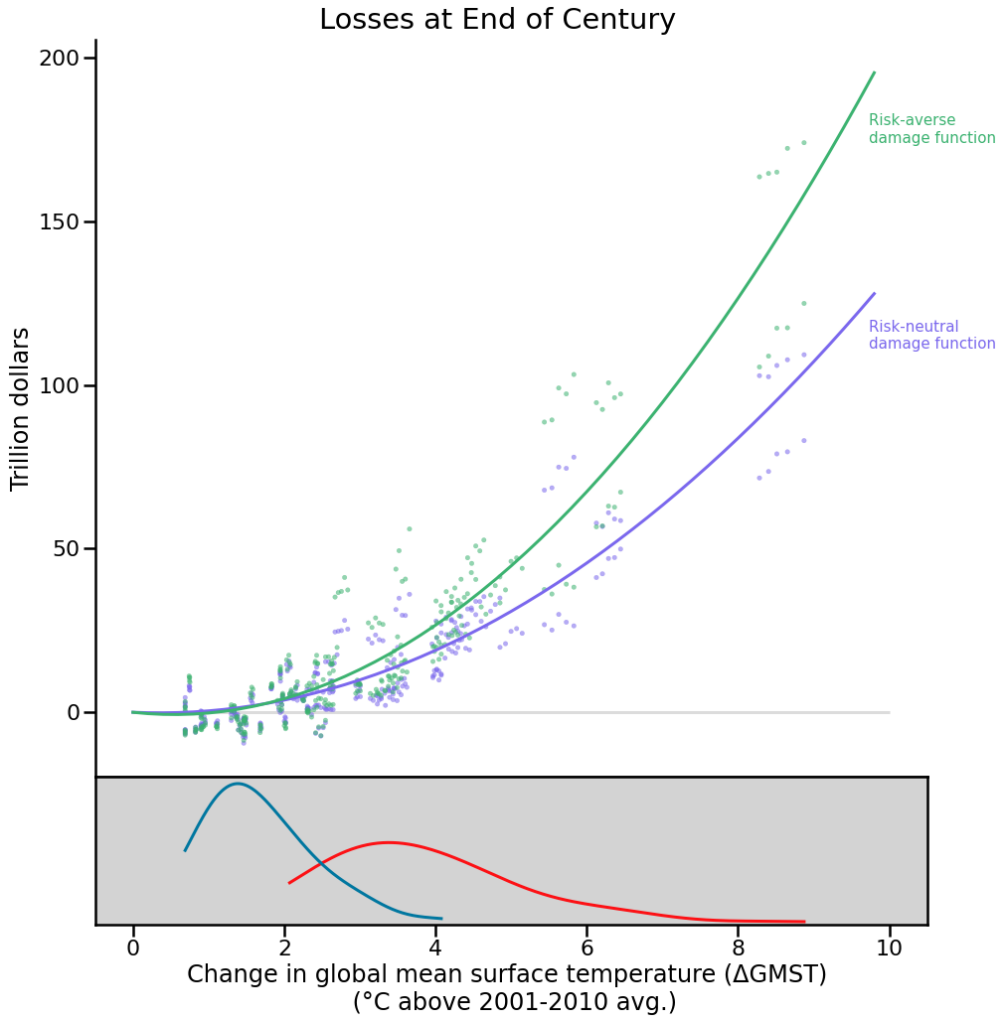

Figure 5: Illustrative damage functions with and without risk aversion Illustration of a damage function estimation with and without risk aversion in underlying spatially aggregated damages. Each data point represents globally aggregated damages from a single GCM-RCP-SSP-growthmodel for a 5 year period at the end of the century, plotted against that GCM-RCP's global average temperature at the end of the century. The green curve is estimated using the green dots, each of which represents a GCM realization of globally-aggregated risk-averse damages. The blue curve is estimated through the blue dots, each of which represents a GCM realization of globally-aggregated risk-neutral damages.

B Appendix: Damage Function Emulation

Climate damages are initially calculated for a small number of socioeconomic scenarios, consisting of SSP trajectories for SSP2, SSP3, and SSP4, as produced by the OECD Env-Growth model and the IIASA GDP model (6 scenarios total). To evaluate damages across the full range of RFF-SPs, we apply an emulation scheme. Conceptually, this scheme interpolates between the SSPs in order to match the country-level GDPs designated by a given RFF-SP.

The emulation scheme is estimated and applied separately for each 5-year period, t, of each RFF-SP, k. For target period t, we have a snapshot consisting of GDP and population levels for each country according to the RFF-SP and each SSP. Within this period, we describe the RFF-SP country-level incomes levels as a unit simplex interpolation of SSP income levels in the same period. That is, we want to select values α_{jkt} for which

$$\text{RFFLogIncome}_{kit} \approx \sum_j \alpha_{jkt} \text{SSPLogIncome}_{jit}$$

for all countries i, across SSP j, such that $\sum_j \alpha_{jkt} = 1$ for each period of each RFF-SP. The natural log of GDP per capita for each country is used, since this is the form of income used in the raw projections. Specifically,

$$\text{RFFLogIncome}_{kit} = \log(\text{RFFGDP}_{kit}/\text{RFFPopulation}_{kit})$$
$$\text{SSPLogIncome}_{jit} = \log(\text{SSPGDP}_{jit}/\text{SSPPopulation}_{jit})$$

using the country-level GDP and population from the RFF-SPs and SSPs.

Since an exact solution is generally not possible, we minimize a weighted sum of country-level errors according to the following optimization problem for each RFF-SP scenario and period:

$$\begin{aligned} \min_{\{\alpha_{jkt}\}} & \sum_i w_{kit} \left| \text{RFFLogIncome}_{kit} - \left(\sum_j \alpha_{jkt} \text{SSPLogIncome}_{jit} \right) \right| \\ \text{such that } & \sum_j \alpha_{jkt} = 1, \\ & \alpha_{jkt} \geq 0 \qquad \forall j \end{aligned}$$

The weighting values, w_{kit}, are set equal to the RFF-SP GDP level for the given country. This allows the optimization to produce a result closer to global GDP. The optimization is solved with linear programming using the Gurobi optimizer (*29*).

Next, we apply the coefficients from the unit simplex interpolation to global damage functions, which we estimated for each SSP within each period, to construct an interpolated damage function. The SSP damage functions are normalized by the global SSP GDP in this step, and then these fractional damages are

multiplied by global RFF GDP to recover level damages. As a result, total damages for RFF-SPs beyond the range of the SSPs are extrapolated linearly. That is, given the SSP-specific damage functions, $d_{jt}(\Delta GMST)$, providing dollar damages in period t as a function of climatic temperature, we calculate

$$d'_{kt}(\Delta\text{GMST}) = \text{RFFGlobalGDP}_{kt} \sum_j \alpha_{jkt}{}^{d_{jt}(\Delta\text{GMST})/\text{SSPGlobalGDP}_{jt}}$$

where $\text{SSPGlobalGDP}_{jt} = \sum_i \text{SSPGDP}_{jit}$ and $\text{RFFGlobalGDP}_{kt} = \sum_i \text{RFFGDP}_{kit}$.

C Appendix: Sector-specific Damages Details

Each sector has different data and method requirements for dose response estimation and projection, and damage function estimation. A description of sector-specific details is included in the following sub-sections.

C.1 Mortality

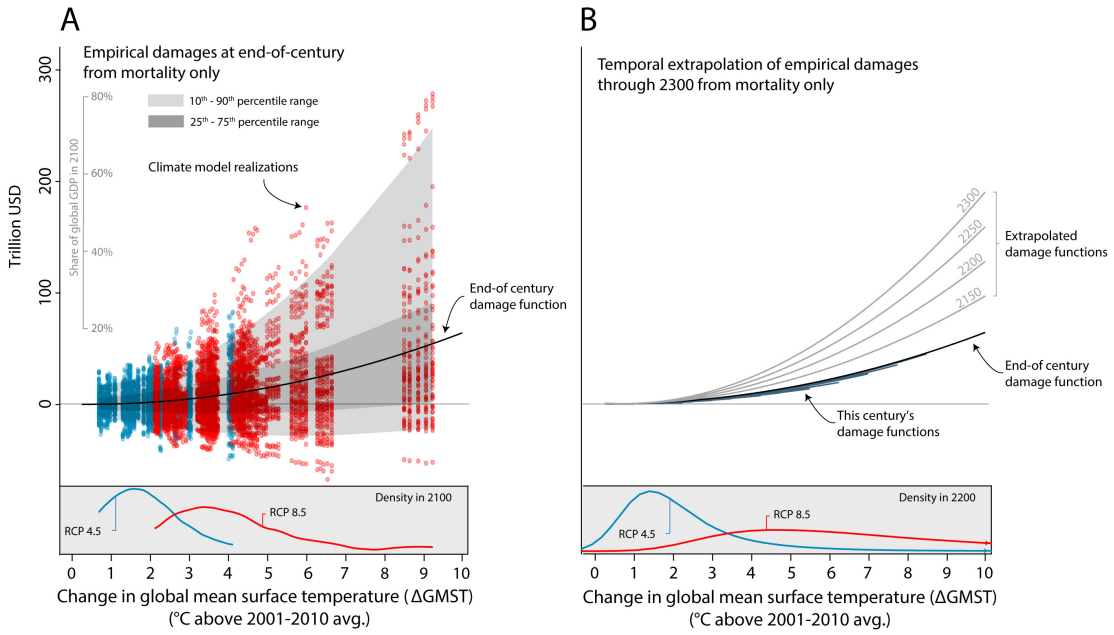

Figure 6: Empirically derived mortality-only damage functions Both panels show damage functions relating empirically derived total global mortality damages to anomalies in global mean surface temperature (ΔGMST) under socioeconomic scenario SSP3. In panel A, each point (red = RCP8.5, blue = RCP4.5) indicates the value of the full mortality risk of climate change in a single year (ranging from 2095 to 2100) for a single simulation of a single climate model, accounting for both costs and benefits of adaptation. The black line is the quadratic damage function estimated through these points. The distribution of temperature anomalies at end of century (2095-2100) under two emissions scenarios across our 33 climate models is in the bottom panel. In panel B, the end-of-century damage function is repeated. Damage functions are shown in dark blue for every 10 years pre-2100, each of which is estimated analogously to the end-of-century damage function and is shown covering the support of ΔGMST values observed in the SMME climate models for the associated year. Our projection results generate mortality damages only through 2100, due to limited availability of climate and socioeconomic projections for years beyond that date. To capture impacts after 2100, we extrapolate observed changes in damages over the 21^{st} century to generate time-varying damage functions through 2300. The resulting damage functions are shown in light grey for every 50 years post-2100, each of which is extrapolated. The distribution of temperature anomalies around 2200 (2181-2200) under two emissions scenarios using the FaIR simple climate model is in the bottom panel. To value lives lost or saved, in both panels we use the age-varying U.S. EPA VSL and an income elasticity of one applied to all impact regions.

- We use comprehensive historical mortality records to quantify how death rates across the globe have been affected by observed climate changes. Specifically, we compile the largest sub-national vital statistics database in the world, detailing 399 million deaths across 41 countries accounting for 55 percent of the global population. These mortality records are combined with decades of detailed daily and local temperature observations.

- We econometrically estimate the relationship that extreme cold and extreme heat have on death rates

in the historical data. We find that the mortality-temperature relationship is strongly modified by the climate and income levels of the affected population, demonstrating that adaptation affects the vulnerability of a population to extreme temperatures.

- We use these empirical mortality-temperature relationships to generate projections of the future impacts of climate change on mortality rates for areas across the globe, dividing the world into 24,378 distinct regions (each containing roughly 300,000 people, about the size of a U.S. county) up to 2100. These projections account for the benefits of adaptation by allowing mortality-temperature relationships to evolve into the future as climates warm and incomes rise.

- We develop a technique to estimate the cost of adaptive behaviors and technologies (*4*). When combined with projections of mortality effects of climate change including adaptation benefits, these projections capture the full mortality risk of climate change, for the first time accounting for both adaptation benefits and costs, in addition to direct mortality impacts.

- Projected impacts of the full mortality risk of climate change are then monetized and used to determine the costs of excess mortality risk in a given year. This monetization uses the U.S. EPA value of a statistical life (VSL), and applies an income elasticity of one to scale the VSL across the globe, using country-level incomes.[54]

- These projections include five scenarios for future income and population growth, two trajectories of future greenhouse gas emissions, and simulations from 33 climate models, allowing for an assessment of the uncertainty surrounding any particular projection. The full estimates also reflect statistical uncertainty related to the underlying economic and health data.

- For a detailed description of the methods and results summarized above, please see Carleton et al (2022) (*4*).

C.2 Energy

- We match globally representative, longitudinal data on energy consumption with $0.25° \times 0.25°$ globally harmonized historical climate data. Energy consumption data are derived from International Energy Agency (IEA) data files that describe electricity and direct fuel consumption across residential, commercial, industrial, and agricultural end-uses (excluding transportation) in 146 countries during 1971-2010.

[54]The U.S. EPA's VSL for 2020 amounts to \$9,926,524.56 (2019\$). Starting from the original published VSL (1990 VSL = \$4.8mil (1990\$)) and following the methodology described in the 2010 EPA Guidelines, the 1990 VSL was adjusted for inflation to the dollar year of DSCIM (2019\$) using the annual GDP deflator and adjusted over time to a 2020 EPA VSL using an IEVSL = 0.4 and income data (real GDP per capita) from the most recent annual FRED series.

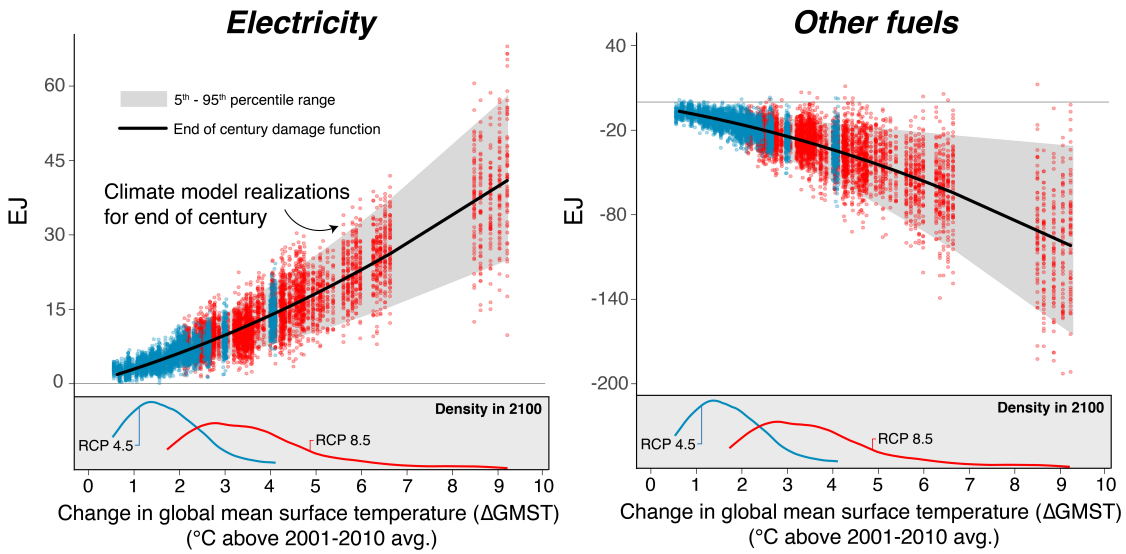

Figure 7: Empirically derived global energy damage functions Total global electricity consumption impacts (left) and other fuels consumption impacts (right) at end-of-century, indexed against ΔGMST realized in each climate model simulation (blue dots=RCP 4.5; red dots=RCP 8.5). Black lines represent end-of-century quadratic damage functions, which are estimated through the points shown. Shaded areas indicate the range between 5^{th} and 95^{th} percentiles. Probability density functions display the distribution of ΔGMST at end-of-century in each emissions scenario.

- We econometrically estimate the effect of historical temperature distributions on national annual per capita energy consumption using random year-to-year variation, and measure how this *energy-temperature response* differs across energy types (*electricity* and *other fuels*), income levels, and climate zones.

- We project impacts of climate change in 24,378 globally comprehensive geographic regions (roughly the size of US counties) through 2099 by combining the econometric results with a probabilistic ensemble of downscaled climate projections based on CMIP5 models. When projecting these impacts, we account for how the energy-temperature response will evolve as populations become richer and exposed to warmer climates.

- We monetize and pool the empirically derived impact projections, aggregating damages across locations and indexing them against the global mean surface temperature anomaly (ΔGMST) expressed in each climate model realization. Damages are projected under five scenarios for future income and population growth, two trajectories of future greenhouse gas emissions, and simulations from 33 climate models, allowing for an assessment of the uncertainty surrounding any particular projection. The full estimates also reflect statistical uncertainty related to the underlying energy-temperature response estimates.

- To monetize the projected impacts of climate change on energy consumption, we apply country-specific real prices for electricity and other fuels to the projected quantity impacts, thus reflecting differential costs across geographies and fuels.

- Impacts on electricity consumption are valued using an average cost of electricity generation, which the IEA's *World Energy Outlook 2017* provides globally as of 2016 at the country or world region level.[55] Impacts on other fuels consumption are valued using residential and non-residential end-user prices excluding taxes, which the IEA's *Energy Prices and Taxes* dataset provides for coal, oil, and natural gas fuels in 55 countries as of 2012.[56] Countries that lack price data for a given fuel are assigned the global average price for that fuel. To obtain a price for the pooled, multi-fuel "other fuels" category, we weight the prices of the individual fuels according to their shares in a country's overall "other fuels" consumption as of 2012 (the most recent year for which consumption data are available).[57] Thus, each country receives unique prices at which its impacts on other fuels consumption are valued.[58]

- To extrapolate prices into the future, we use US average annual price growth rates for electricity and other fuels between 2020 and 2050, as projected by the US Energy Information Administration's *Annual Energy Outlook 2021* (AEO). We apply these growth rates up to the year 2099 to the baseline country $\times$ fuel prices described above. Specifically, based on AEO projections, we allow electricity prices to decline by 0.27% per year and other fuels prices to rise by 0.82% per year.[59]

- For a detailed description of the methods and results summarized above, please see Rode et al. (2021) (*3*), which is published at *Nature*.

C.3 Labor Supply

- We harmonize daily and weekly worker-level labor supply data from time use and labor force surveys in seven countries (USA, Mexico, Brazil, France, UK, Spain, and India) and combine these data with detailed daily and local temperature observations.

- We systematically evaluate the nonlinear response of labor supply to daily temperature separately for workers in "high-risk" sectors (i.e., weather-exposed sectors– agriculture, mining, construction, and manufacturing) and low-risk sectors (all others).

[55] Costs are specified for the following geographies: Japan, European Union, Korea, Brazil, Australia, Mexico, Southeast Asia, Middle East, India, Africa, United States, China, Canada, Russia. When a cost is not available specific to a particular geography we extend these costs based on UN world region classifications: Oceania receives the Australia cost, N., S., and W. Europe receive the EU cost, E. Europe receives the Russia cost, Central America/Caribbean receive the Mexico cost, S. America receives the Brazil cost, N. Africa receives the Middle East cost, and S. Asia receives the India cost.

[56] We take a weighted average of residential and non-residential prices, with a weight of 16% on residential and 84% on non-residential. These weights are determined based on the average share of consumption in these two sectors in the set of 55 countries where a sectoral breakdown is available.

[57] Although our consumption data do cover fuels besides coal, oil, and natural gas (including solar, geothermal, and biofuels), no price data are available for fuels other than coal, oil, and natural gas. We therefore extend the weighted average price to the remaining fuels.

[58] Even countries that are assigned the global average price for the individual fuels will differ in the shares of each fuel in their other fuels consumption mix.

[59] The electricity price growth rate is of a consumption-weighted average electricity price across residential, commercial, and industrial sectors. The other fuels price growth rate is of a consumption-weighted average price across multiple fuels (i.e., natural gas, metallurgical coal, other coal, coal to liquids, distillate fuel oil, residual fuel oil, propane, and motor gasoline) in residential, commercial, and industrial sectors.

- We apply these labor supply-temperature responses over novel probabilistic climate change projections to project the effects of climate change on the labor supply of high- and low-risk workers in each of 24,378 impact regions. Importantly, in characterizing total impacts in each region, we take into account the changing composition of its workforce over time across high- and low-risk workers. Future shares of high- and low-risk workers are predicted based on present-day empirical estimates of how these shares vary as a function of income and average climate, together with high-resolution data on future incomes and climates.

- Interpreting labor supply impacts of climate change through a simple theoretical framework, we monetize the implied disutility to workers of a warmer climate, following the method in Rode et al. (2021) (*22*). This monetized value is calculated in terms of the compensating wage increase needed to offset the implied disutility due to warming, which is revealed by the labor supply response of workers to warmer temperatures.

- We aggregate projected monetized disutility costs (i.e., damages) across all workers in all locations globally to obtain total global damages. Damages are projected under five scenarios for future income and population growth, two trajectories of future greenhouse gas emissions, and simulations from 33 climate models, allowing for an assessment of the uncertainty surrounding any particular projection. The full estimates also reflect statistical uncertainty related to the underlying dose-response function estimates.

- For a detailed description of the methods and results summarized above, please see Rode et al (2022) (*22*).

C.4 Agricultural Productivity

- We assemble one of the largest datasets of subnational crop production available to researchers, constructing a dataset for six crops in 12,658 locations (41,186 location-crop pairs) in 55 countries spanning up to 137 years. We cover the staple crops maize, soybean, rice, wheat, cassava, and sorghum; representing two thirds of global crop caloric production. These data are drawn from individual country sources for each country and span varying numbers of years. Full details can be found in (*23*).

- A key issue is determining what weather variables are important for future crop yields, as a wide range of candidate weather measures has been proposed in the literature, but debate has continued over which are of first-order importance. These include, for example, vapor pressure deficit, degree days, minimum temperature, drought, the count of rainy days, and the total amount of extreme rainfall. We adapt cross-validation, a machine learning technique, to a causal inference context, enabling us to systematically assess a rich set of channels through which weather shocks might causally affect yields

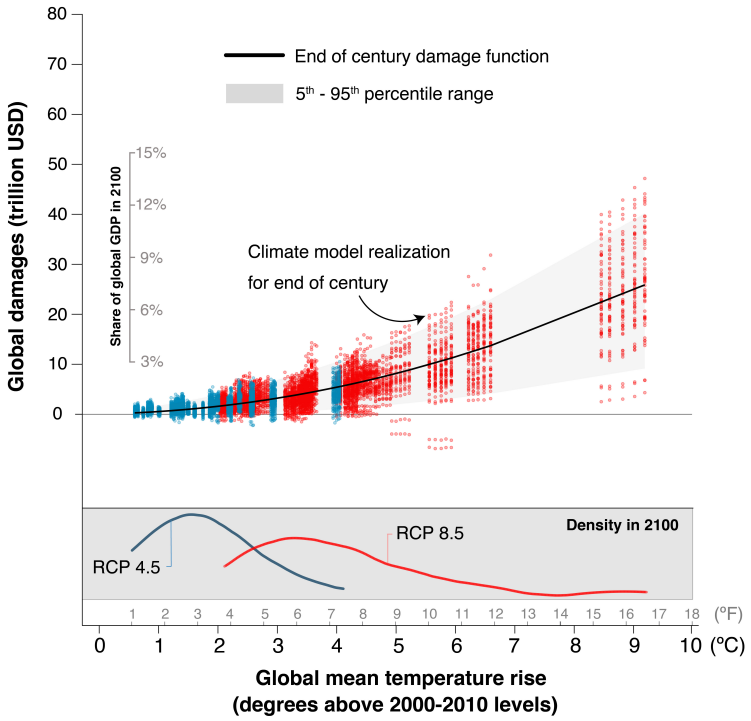

Figure 8: Empirically derived labor supply damage function The damage function above relates empirically derived total global labor disutility damages to anomalies in global mean surface temperature (ΔGMST) at end-of-century. Each point (red = RCP8.5, blue = RCP4.5) indicates the global labor disutility costs of climate change in a single year (ranging from 2095 to 2099) for a single simulation of a single climate model, accounting for changes to workforce composition as incomes grow and the climate warms. The black line represents the end-of-century quadratic damage function, which is estimated through the points shown. Shaded areas indicate the range between 5^{th} and 95^{th} percentiles. Probability density functions display the distribution of ΔGMST at end-of-century in each emissions scenario.

in each of our crops, while also systematically assessing the extent to which farmers might use access to income, irrigation, or expectations of long-run climate to mitigate these yield losses.

- We account for adaptation (*30*) by observing the real world trade-offs that farmers make as they are confronted with different climates under different socioeconomic conditions, and estimate implied adaptation costs (*4*) assuming a profit-maximizing farmer.

- Following (*4*), we use our empirically based, adaptation-adjusted yield-temperature and yield-precipitation relationships to generate projections of the future impacts of climate change on crop yields for areas across the globe, dividing the world into 24,378 distinct regions (each containing roughly 300,000 people, about the size of a U.S. county) up to the end of the 21^{st} century.

- We develop an approach to value changes in future global yields under climate change. To do this, we assign country-specific average prices to total calorie production, allowing producers to intensify or reduce production in order to meet demand in their market at increasing marginal cost. In general, aggregate yield losses under climate change harm consumers as caloric consumption is lower and prices are higher; producers are also harmed by production losses, but this harm may be offset by profit gains

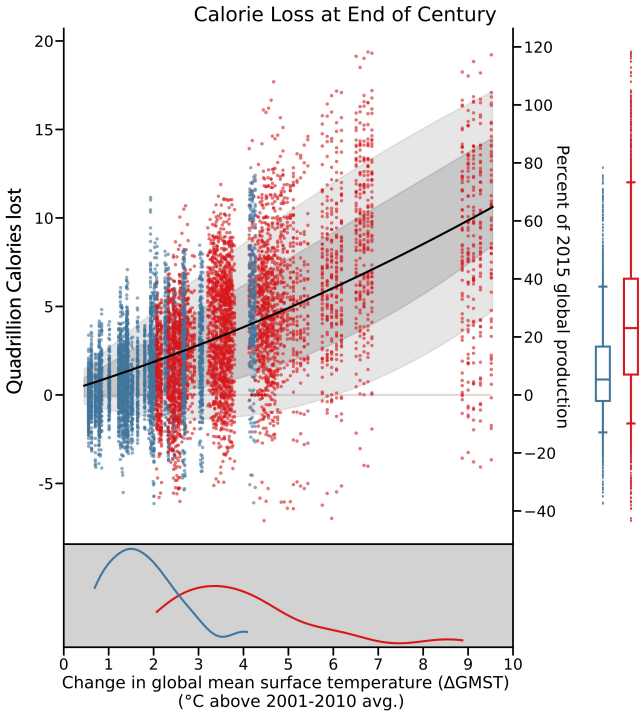

Figure 9: Empirically derived agriculture damage function Empirical damage function describing calories (kCal) lost as a quadratic function of the global mean surface temperature anomaly (Δ GMST). Each point represents a single climate-model-by-Monte-Carlo run for RCP 4.5 (blue) or RCP 8.5 (red) in 2093-2097. Grey bands indicate quantiles 10-90 and 25-75, conditional on Δ GMST. The bottom panel shows the distribution of warming under each RCP, boxplots to the right show the distribution of end-of-century damages by RCP. The right axis describes end-of-century caloric losses normalized by 2015 global caloric production of the six crops studied here (maize, soybean, rice, wheat, cassava, and sorghum).

from higher prices. All estimates and projections of yield impacts account for within-crop varietal switching. In monetizing these yield impacts, we additionally account for costly changes in the total amount of agricultural land (along a long-run supply curve) in response to price signals caused by net changes to the overall supply of staple crops under climate change. This movement along the long-run supply curve is in response to the price signal from slow moving (and therefore expected) changes in supply in-line with climate change; annual weather deviations from the long-run trend are unexpected and occur after planting decisions have been made, so farmers cannot respond to this component of the price signal. We apply a simple shrinkage estimator to the variance in prices to account for the price and quantity effects of storage. Consumers demand calories with perfect substitution between crops, with the distribution of cropped locations and crop types held fixed. Trade is assumed to be frictionless within set markets, and zero between these markets.

- As a last step in the valuation process, the results are multiplied by 0.45 to account for crop switching and global trade protective effects, based on an average of the estimates in prior research documenting these quantities (e.g., (*31*); (*32*); (*33*); (*34*)). The DSCIM-EPA results also account for the benefits of CO_2 fertilization on crop yields based on established estimates in the literature (Moore et al., 2017).

Based on the various scenarios presented in (*23*), CO_2 fertilization is generally found to affect crop yields by 5.0-9.5% and monetized damages by less than 5%.

- For a detailed description of the methods and results summarized above, please see (*23*).

C.5 Coastal

Our sea level rise impact projections rely on outputs from pyCIAM, a model derived from the Coastal Impact and Adaptation Model (CIAM, (*35*)) and modified with updated input data, improved process representation, and increased scalability (*27*). The functionality of that model is described in (*27*), though inputs used in that manuscript differ slightly from those used in this version of DSCIM, due to the need to ensure consistency in input data across sectors. Below, we briefly describe the data inputs used in this version:

- We create a global model of coastal dryland and wetland area, historical population, and physical capital by coastline segment and 10cm elevation bins. We do so by aggregating best-available high-resolution global datasets describing capital distribution (LitPop v1.2, (*36*)), population (Landscan 2011, (*37*)), coastal elevation (CoastalDEM v1.1, (*38*)), and wetland/mangrove extent (GLOBCOVER v2.3, (*39*); Global Mangrove Watch 2016 (*40*)).

- We augment these data with estimates of Local Mean Sea Level (LMSL, AVISO+ Mean Dynamic Topography, (*41*)) and extreme sea level (ESL) distributions (CoDEC, (*42*)). These data combined allow for the representation of historical flood exposure.

- To model future exposure consistent with the SSPs, we estimate local SLR using the LocalizeSL model (v3.2, (*43*, *44*))[60] and population and income using the downscaled SSP income dataset following the common approach used across sectors (e.g. (*4*, *3*)). Furthermore, we leverage the capital growth model contained within the OECD Env-Growth model (*24*) to project country-level trends in physical capital. These country-level trends are used to scale segment-by-elevation capital stock data over time.

- Current and projected future representations of exposure (land area, physical capital, and population) and hazard (SLR and extreme sea levels) are aggregated into a single dataset - the Sea Level Impacts Input Dataset by Elevation, Region, and Scenarios (SLIIDERS) dataset (*27*).[61] Dryland and wetland values are estimated from country-level income and local population density (for dryland value), based on the corresponding equations in (*27*) (derived from (*35*)). The fraction of each country's capital stock that is mobile is estimated from capital class categorizations in Penn World Table 10.0 (*45*). Country-level construction costs are taken from the 2021 World Bank International Comparison Project (ICP)

[60] Available at: https://github.com/bobkopp/LocalizeSL

[61] The dataset used in the DSCIM model described here differs slightly from the dataset released with this manuscript, to ensure consistency in socioeconomic data across all DSCIM sectors

(*46*) and augmented with data from (*47*) for countries not appearing in the ICP. A country-level resilience factor used in CIAM is updated based on downscaled income. Country-level VSL values are used internally within the optimal adaptation model to value extreme sea level-driven mortality when determining an optimal adaptation pathway. Country-level VSL is also used when valuing mortality impacts along that optimal pathway.

- pyCIAM estimates protection and retreat strategies, as well as incurred costs, for a set of mutually exclusive global coastal segments. We use a set of 9,096 segments (19,714 unique intersections of coastal segment and impact region) based on the locations at which extreme sea levels are estimated in the CoDEC input dataset. Costs are divided into those arising from managed and unmanaged retreat, dryland lost to inundation, wetland lost to inundation and protective barriers, construction and maintenance of those protections, and life and property lost due to storm surge. The specification of internal functions used to estimate these various cost types and to determine optimal adaptation strategy by segment are described in detail in (*27*).

- We run pyCIAM on the three SSP scenarios (using the two growth models to project capital stock and income)[62]; 11 SLR scenarios based on the CMIP5 RCP emissions pathways[63] and various assumptions of sea level dynamics; and 10,000 Monte Carlo samples to represent the distribution of possible local mean sea level (LMSL) values conditional on each of those scenarios. This results in 660 thousand unique simulations of coastal costs and adaptation under different future trajectories of hazard and exposure (110,000 SLR trajectories and 6 socioeconomic trajectories). We additionally run the model for 10,000 Monte Carlo samples representing background LMSL change in the absence of climate change. This background change includes factors such as Glacial Isostatic Adjustment (GIA), tectonics, and subsidence. The difference in projected average annual loss (AAL) between each "with climate change" sample and the corresponding "without climate change" sample defines the sea level rise-attributable damages for that Monte Carlo draw.

- We then group the 110,000 SLR realizations based on their GMSL value in each year to create a conditional distribution of possible coastal damages as a function of year and GMSL, for each choice of socioeconomic trajectory. These estimates are then used to construct coastal damage functions relating damages to GMSL, identically to how damage functions relating damages to GMST are constructed for other sectors.

- To model damages from a GHG pulse, we need to model the impact of that pulse on GMSL. To do this, the NASEM "Valuing Climate Damages" report suggested the use of semi-empirical models to

[62] (*27*) incorporate 5 SSP scenarios, however due to cross-sectoral consistency, only 3 are used here.

[63] CMIP5 RCP emissions pathways are used in the LocalizeSL modeling, however the remainder of the DSCIM coastal sector relies on CMIP6 RCP emissions pathways. Unless otherwise specified, "RCP" in this section refers to CMIP6 emissions scenarios. This is meant to avoid confusion between the naming of the SSP socioeconomic pathways and the "SSP-RCP" (e.g. "SSP3-7.0") nomenclature used in CMIP6 representative concentration pathway emissions pathways.

define the statistical relationship between GMST and GMSL (*1*). We use the model shown as an example in that report, appropriately titled the Semi-Empirical Sea Level (SESL) model (*48*), which is calibrated to geological evidence about the relationship between GMST and GMSL over the last two thousand years. We run this model on the FaIR GMST outputs both with and without a GHG pulse to generate an equivalent number of GMSL realizations. We subtract the runs without the pulse from the runs with the pulse to determine the impact of the pulse on GMSL. We then add this distribution of GMSL pulse differences to baseline probabilistic projections of GMSL, modeled using the Framework for Assessing Changes to Sea-level (FACTS) as described in the IPCC's 2021 Sixth Assessment Report (AR6) (*21*, *49*). We align this distribution of baseline GMSL with that of the GHG pulse-induced marginal SLR by quantile mapping the SESL outputs under the control experiment (i.e. no pulse) with the FACTS-based distribution in each year and for each RCP. For example, the pulse associated with the 60th percentile of GMSL in 2050 for RCP7.0[64] under the control scenario is added to the 60th percentile of RCP7.0 projections in 2050 from FACTS. This quantile mapping is defined mathematically as:

$$\tilde{h}_{\text{base},r,y,p} = \text{ppf}\left(\mathbf{h}_{\text{FACTS},r,y}, \text{cdf}\left(\mathbf{h}_{\text{SESL}_{\text{base}},r,y}, h_{\text{SESL}_{\text{base}},r,y,p}\right)\right) \tag{20}$$

$$\tilde{h}_{\text{pulse},r,y,p} = \tilde{h}_{\text{base},r,y,p} + h_{\text{SESL}_{\text{pulse}},r,y,p} - h_{\text{SESL}_{\text{base}},r,y,p} \tag{21}$$

where

- $\tilde{h}_{\text{base/pulse},r,y,p}$ are the bias-corrected GMSL projections for scenarios without (base) and with (pulse) a GHG pulse, for RCP scenario r, in year y, using draw p from the distributions of climate and sea level parameters characterizing FaIR and SESL, respectively;
- $h_{SESL_{\text{base}},r,y,p}$ is the SESL-based GMSL projection for the same indices of RCP, year, and parameter draw;
- $\mathbf{h}_{m,r,y} = \begin{bmatrix} h_{m,r,y,1} \\ h_{m,r,y,2} \\ \dots \\ h_{m,r,y,n_p} \end{bmatrix}$ is the full distribution of GMSL projections for model m (either FACTS or $\text{SESL}_{\text{base}}$) across all n_p climate and sea level parameter draws;
- $\text{cdf}(\mathbf{d}, v)$ is the empirical cumulative distribution function for distribution $\mathbf{d}$ and value v; and
- $\text{ppf}(\mathbf{d}, q)$ is the percent point function (inverse cdf) for distribution $\mathbf{d}$ and quantile q

The bias correction of SESL-based GMSL values to the distribution seen in the IPCC AR6 ensures consistency with the best available assessment of projected future sea-level rise. Notably, however,

[64] We use "RCP7.0" to replace the CMIP6 nomenclature of "SSP3-7.0" to avoid confusion with the SSP socioeconomic pathways.

our use of the FACTS AR6 projections differs from the presentation in AR6 in a few respects that makes overall GMSL projections more conservative (both slightly lower and narrower). First, AR6 presents 'p-boxes' that characterize *imprecise* probabilities, produced by combining multiple probability distributions of sea-level change for the same forcing. Such p-boxes take the outer limits of all the probability distributions considered. For example, the *likely* range in AR6 has *at least* a 66% probability of containing the true value. Such imprecise probabilities are ill-suited for benefit-cost analyses, and so instead we combine the contributing probability distributions using equal weights. This will lead the resulting distributions to be narrower than those presented in AR6. Second, while AR6 focuses upon *medium confidence* projections that consider only those ice-sheet processes for which there is at least a medium level of evidence with medium agreement, they also consider, in parallel, projections that incorporate processes in which there is *low confidence* (limited evidence and/or low agreement) regarding magnitude, rate, timing and thresholds (see AR6 WG1, Box 9.4). Our projections are based upon the AR6 *medium confidence* projections exclusively, and so do not consider, for example, potential contributions from Marine Ice Cliff Instability. Finally, like our projections, AR6's *medium confidence* projections from 2100 to 2150 are based upon the assumption on no additional ice-sheet acceleration after 2100; however, beyond 2150, there is *low confidence* in all projections, and so AR6 combines multiple additional methods to project GMSL rise in 2300. Our projections through 2300 are consistent with the approach adopted by AR6 through 2150 and do not incorporate these alternate methods, leading our 2300 projections under SSP5-8.5 to be lower and narrower than those emphasized in AR6 (e.g. in AR6 WG1, Fig. SPM.8).

- The FACTS-based baseline GMSL trajectories are only available for the CMIP6 RCP emissions trajectories. To approximate baselines for each of the 10,000 RFF-SP GMSL scenarios (10,000 joint draws of RFF-SP and FaIR/SESL climate parameters), we employ a 3-step process:

    1. For each year, y, of the projection, we search for the two "bounding" RCP scenarios, r_{low} and r_{hi}. To do this, we first identify the FAIR/SESL parameter draw, p_s, associated with this RFF-SP draw, s, and find the corresponding SESL-based GMSL projection, $h_{\text{SESL}_{base},\text{RFF-SP}_s,y,p_s}$. We then find the SESL-based GMSL projections associated with each of the RCPs for the given year and parameter draw, $h_{\text{SESL}_{base},r,y,p_s}$. We find the two RCPs, r_{low} and r_{hi}, with GMSLs that most closely bound that of the RFF-SP draw, conditional on the selection of p_s. We assign weights to these RCPs according to their relative distance from the RFF-SP. For example, suppose RFF-SP_{10} has a projected GMSL of 0.78 m in 2100. Using FAIR/SESL parameter set p_{10}, if RCP4.5 and RCP7.0 are the closest bounding scenarios with projections of 0.7m and 0.8m in 2100, we would assign $w_{RCP4.5} = 0.2$ and $w_{RCP7.0} = 0.8$ for RFF-SP_{10} in 2100. See Figure 10a.[65]

[65] When the SESL-based GMSL for a given y and p falls outside of the bounds of GMSL across all RCP, we simply assign unit weight to the nearest RCP.

2. For both r_{low} and r_{hi} we perform a quantile mapping from the SESL-based and FACTS-based GMSL distributions using Equation 20, with a lookup value defined by the SESL-based GMSL projection for the given RFF-SP scenario in the given year and with the given parameter draw (0.78 m in the previous example). This yields us two bias-corrected representations of this value, each derived from one of the bounding RCPs. See Figure 10b.

3. We take the weighted average of the two bias-corrected GMSL estimates, using the weights from Step 1. See Figure 10c.

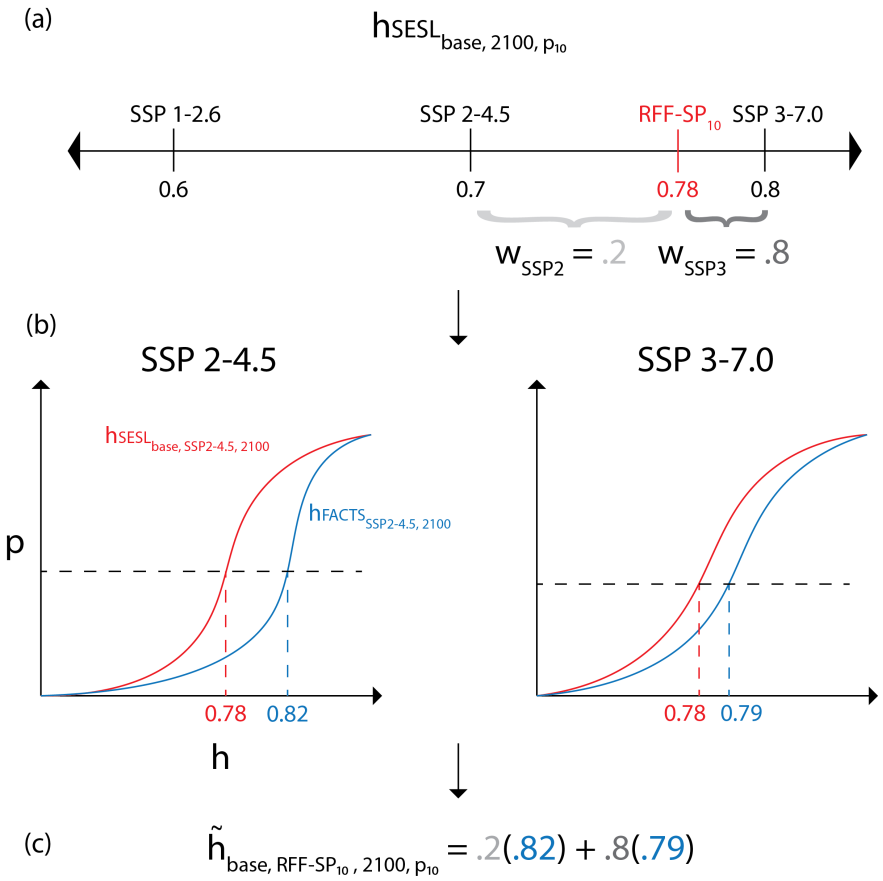

Figure 10: Schematic of GMSL Projection Approach This figure illustrates the process to bias-correct Semi-Empirical Sea Level projections for the RFF-SPs. In (a), we determine the bounding SSP-RCPs for a given RFF-SP, year, and FAIR/SESL parameter draw. The figure uses 10 as an example RFF-SP draw index, matched to a FAIR/SESL parameter draw with the same index. Only three SSP-RCPs are shown for illustration. In (b), we quantile map from the SESL-based GMSL projections to the FACTS-based GMSL projections for each of the two bounding SSP-RCPs. In (c), we take the weighted average of the two quantile mapped projections.

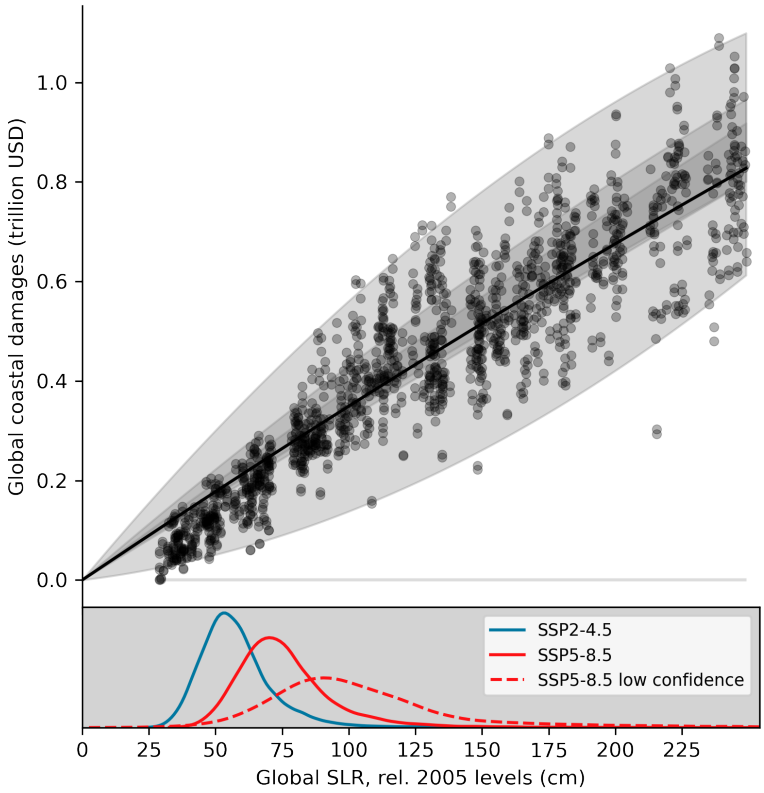

Figure 11: Model-derived coastal damage function Damage function describing aggregate economic losses due to sea level rise as a function of the global mean sea level anomaly (Δ GMSL). Each point represents the average annual loss calculated from a single realization of local mean sea levels (LMSLs) consistent with the associated GMSL value in the 2085-2105 period (centered on 2095). These GMSL values are relative to the GMSL in 1990-2010. The black line indicates the damage function defined by Ordinary Least Squares (OLS) regression, while grey bands display quantile regression results for quantiles 1-99, 10-90, and 25-75. Damages arise from land value loss, storm surge-driven mortality and capital stock losses, domestic migration, construction of local protections, and wetland loss. They are estimated separately for 9,500 unique coastal segments using the CIAM model. The bottom panel shows the distribution under SSP2-4.5, SSP5-8.5, and a low-likelihood, high-consequence scenario involving plausible ice sheet dynamics that lead to high GMSL values when coupled with the SSP5-8.5 emissions trajectory.

References

[1] N. A. of Sciences Engineering and Medicine, *Valuing Climate Damages: Updating Estimation of the Social Cost of Carbon Dioxide*. Washington, DC: The National Academies Press, 2017.

[2] T. Carleton and M. Greenstone, "A guide to updating the us government's social cost of carbon," *Review of Environmental Economics and Policy*, vol. 16, no. 2, pp. 196–218, 2022.

[3] A. Rode, T. Carleton, M. Delgado, D. Gergel, M. Greenstone, T. Houser, S. Hsiang, A. Hultgren, A. Jina, R. E. Kopp, K. E. McCusker, I. Nath, J. Rising, and Y. Jiacan, "Estimating a social cost of carbon for global energy consumption," *Nature*, 2021.

[4] T. Carleton, A. Jina, M. Delgado, M. Greenstone, T. Houser, S. Hsiang, A. Hultgren, R. E. Kopp, K. E. McCusker, I. Nath, J. Rising, A. Rode, H. K. Seo, A. Viaene, J. Yuan, and A. T. Zhang, "Valuing the Global Mortality Consequences of Climate Change Accounting for Adaptation Costs and Benefits*," *The Quarterly Journal of Economics*, vol. 137, pp. 2037–2105, 04 2022.

[5] S. Hsiang, R. Kopp, A. Jina, J. Rising, M. Delgado, S. Mohan, D. Rasmussen, R. Muir-Wood, P. Wilson, M. Oppenheimer, K. Larsen, and T. Houser, "Estimating economic damage from climate change in the United States," *Science*, vol. 356, no. 6345, pp. 1362–1369, 2017.

[6] N. Gennaioli, R. L. Porta, F. L. D. Silanes, and A. Shleifer, "Growth in regions," *Journal of Economic Growth*, vol. 19, pp. 259–309, September 2014.

[7] Eurostat, *Europe in Figures: Eurostat Yearbook 2013*. Publications Office of the European Union, 2013.

[8] K. Riahi, D. P. Van Vuuren, E. Kriegler, J. Edmonds, B. C. O'neill, S. Fujimori, N. Bauer, K. Calvin, R. Dellink, O. Fricko, *et al.*, "The shared socioeconomic pathways and their energy, land use, and greenhouse gas emissions implications: an overview," *Global Environmental Change*, vol. 42, pp. 153–168, 2017.

[9] U. K. Müller, J. H. Stock, and M. W. Watson, "An econometric model of international long-run growth dynamics," tech. rep., National Bureau of Economic Research, 2019.

[10] K. Rennert, B. C. Prest, W. A. Pizer, R. G. Newell, D. Anthoff, C. Kingdon, L. Rennels, R. Cooke, A. E. Raftery, H. Ševčíková, *et al.*, "The social cost of carbon: Advances in long-term probabilistic projections of population, gdp, emissions, and discount rates," *Brookings Papers on Economic Activity*, 2021.

[11] A. E. Raftery and H. Ševčíková, "Probabilistic population forecasting: Short to very long-term," *International Journal of Forecasting*, 2021.

[12] D. Rasmussen, M. Meinshausen, and R. J. Kopp, "Probability-weighted ensembles of u.s. county-level climate projections for climate risk analysis," *Journal of Applied Meteorology and Climatology*, 2016.

[13] J. Sheffield, G. Goteti, and E. Wood, "Development of a 50-year high-resolution global dataset of meteorological forcings for land surface," *Journal of Climate*, 2006.

[14] B. Thrasher, E. P. Maurer, C. McKellar, and P. B. Duffy, "Technical note: Bias correcting climate model simulated daily temperature extremes with quantile mapping," *Hydrology and Earth System Sciences*, vol. 16, no. 9, pp. 3309–3314, 2012.

[15] K. E. Taylor, R. J. Stouffer, and G. A. Meehl, "An overview of cmip5 and the experiment design," *Bulletin of the American Meteorological Society*, 2012.

[16] A. Wood, L. Leung, V. Sridhar, and D. Lettenmaier, "Hydrologic implications of dynamical and statistical approaches to downscaling climate model outputs," *Climatic Change*, 2004.

[17] R. J. Millar, J. S. Fuglestvedt, P. Friedlingstein, J. Rogelj, M. J. Grubb, H. Damon Matthews, R. B. Skeie, P. M. Forster, D. J. Frame, and M. R. Allen, "Emission budgets and pathways consistent with limiting warming to 1.5° c," *Nature Geoscience*, 2017.

[18] C. J. Smith, R. J. Kramer, G. Myhre, P. M. Forster, B. J. Soden, T. Andrews, O. Boucher, G. Faluvegi, D. Fläschner, Hodnebrog, M. Kasoar, V. Kharin, A. Kirkevåg, J.-F. Lamarque, J. Mülmenstädt, D. Olivié, T. Richardson, B. H. Samset, D. Shindell, P. Stier, T. Takemura, A. Voulgarakis, and D. Watson-Parris, "Understanding rapid adjustments to diverse forcing agents," *Geophysical Research Letters*, vol. 45, no. 21, pp. 12,023–12,031, 2018.

[19] P. Forster, T. Storelvmo, K. Armour, W. Collins, J. L. Dufresne, D. Frame, D. J. Lunt, T. Mauritsen, M. D. Palmer, M. Watanabe, M. Wild, and H. Zhang, "The earth's energy budget, climate feedbacks, and climate sensitivity," in *Climate Change 2021: The Physical Science Basis. Contribution of Working Group I to the Sixth Assessment Report of the Intergovernmental Panel on Climate Change* (V. Masson-Delmotte, P. Zhai, A. Pirani, S. L. Connors, C. Péan, S. Berger, N. Caud, Y. Chen, L. Goldfarb, M. I. Gomis, M. Huang, K. Leitzell, E. Lonnoy, J. B. R. Matthews, T. K. Maycock, T. Waterfield, O. Yelekçi, R. Yu, and B. Zhou, eds.), Cambridge University Press, 2021.

[20] C. Smith, "FaIR v1.6.2 calibrated and constrained parameter set," Sept. 2021.

[21] B. Fox-Kemper, H. T. Hewitt, C. Xiao, G. Aðalgeirsdóttir, S. S. Drijfhout, T. L. Edwards, N. R. Golledge, M. Hemer, R. E. Kopp, G. Krinner, A. Mix, D. Notz, S. Nowicki, I. S. Nurhati, L. Ruiz, J.-B. Sallée, A. B. A. Slangen, and Y. Yu, "Ocean, cryosphere, and sea level change," in *Climate Change 2021: The Physical Science Basis. Contribution of Working Group I to the Sixth Assessment Report of the Intergovernmental Panel on Climate Change* (V. Masson-Delmotte, P. Zhai, A. Pirani, S. L. Connors,

C. Péan, S. Berger, N. Caud, Y. Chen, L. Goldfarb, M. I. Gomis, M. Huang, K. Leitzell, E. Lonnoy, J. B. R. Matthews, T. K. Maycock, T. Waterfield, O. Yelekçi, R. Yu, and B. Zhou, eds.), Cambridge University Press, 2021.

[22] A. Rode, R. E. Baker, T. Carleton, A. D'Agostino, M. Delgado, T. Foreman, D. R. Gergel, M. Greenstone, T. Houser, S. Hsiang, A. Hultgren, A. Jina, R. E. Kopp, S. B. Malevich, K. McCusker, I. Nath, M. Pecenco, J. Rising, and J. Yuan, "Labor disutility in a warmer world: The impact of climate change on the global workforce," *Working Paper*, Sept. 2022.

[23] Hultgren, Andrew and Carleton, Tamma and Delgado, Michael and Gergel, Diana R. and Greenstone, Michael and Houser, Trevor and Hsiang, Solomon and Jina, Amir and Kopp, Robert E. and Malevich, Steven B. and McCusker, Kelly and Mayer, Terin and Nath, Ishan and Rising, James and Rode, Ashwin and Yuan, Jiacan, "Estimating global impacts to agriculture from climate change accounting for adaptation," *Working Paper*, Sept. 2022.

[24] R. Dellink, J. Chateau, E. Lanzi, and B. Magné, "Long-term economic growth projections in the shared socioeconomic pathways," *Global Environmental Change*, 2015.

[25] K. Samir and W. Lutz, "The human core of the shared socioeconomic pathways: Population scenarios by age, sex and level of education for all countries to 2100," *Global Environmental Change*, 2014.

[26] W. K. Viscusi and J. E. Aldy, "The value of a statistical life: a critical review of market estimates throughout the world," *Journal of risk and uncertainty*, vol. 27, no. 1, pp. 5–76, 2003.

[27] N. Depsky, I. Bolliger, D. Allen, J. H. Choi, M. Delgado, M. Greenstone, A. Hamidi, T. Houser, R. E. Kopp, and S. Hsiang, "Dscim-coastal v1.0: An open-source modeling platform for global impacts of sea level rise," *EGUsphere*, vol. 2022, pp. 1–47, 2022.

[28] M. L. Weitzman, "On modeling and interpreting the economics of catastrophic climate change," *Rev. Econ. Stat.*, vol. 91, pp. 1–19, Feb. 2009.

[29] Gurobi Optimization, LLC, "Gurobi Optimizer Reference Manual," 2022.

[30] W. Schlenker, M. J. Roberts, and D. B. Lobell, "US maize adaptability," *Nature Climate Change*, vol. 3, no. 8, pp. 690–691, 2013.

[31] J. Rising and N. Devineni, "Crop switching reduces agricultural losses from climate change in the united states by half under rcp 8.5," *Nature communications*, vol. 11, no. 1, pp. 1–7, 2020.

[32] A. Costinot, D. Donaldson, and C. Smith, "Evolving comparative advantage and the impact of climate change in agricultural markets: Evidence from 1.7 million fields around the world," *Journal of Political Economy*, vol. 124, no. 1, pp. 205–248, 2016.

[33] C. Gouel and D. Laborde, "The crucial role of domestic and international market-mediated adaptation to climate change," *Journal of Environmental Economics and Management*, vol. 106, p. 102408, 2021.

[34] M. Stevanović, A. Popp, H. Lotze-Campen, J. P. Dietrich, C. Müller, M. Bonsch, C. Schmitz, B. L. Bodirsky, F. Humpenöder, and I. Weindl, "The impact of high-end climate change on agricultural welfare," *Science advances*, vol. 2, no. 8, p. e1501452, 2016.

[35] D. B. Diaz, "Estimating global damages from sea level rise with the Coastal Impact and Adaptation Model (CIAM)," *Climatic Change*, vol. 137, pp. 143–156, July 2016. Publisher: Springer Netherlands.

[36] S. Eberenz, D. Stocker, T. Röösli, and D. N. Bresch, "Asset exposure data for global physical risk assessment," *Earth System Science Data*, vol. 12, 4 2020.

[37] J. Graesser, A. Cheriyadat, R. Vatsavai, V. Chandola, J. Long, and E. Bright, "Image based characterization of formal and informal neighborhoods in an urban landscape," *Ieee Journal Of Selected Topics In Applied Earth Observations And Remote Sensing*, vol. 5(4), pp. 1164–1176, 2012.

[38] S. A. Kulp and B. H. Strauss, "CoastalDEM: A global coastal digital elevation model improved from SRTM using a neural network," *Remote Sensing of Environment*, vol. 206, pp. 231–239, 3 2018.

[39] European Space Agency and UCLouvain, "Globcover 2009."

[40] P. Bunting, A. Rosenqvist, R. M. Lucas, L.-M. Rebelo, L. Hilarides, N. Thomas, A. Hardy, T. Itoh, M. Shimada, and C. M. Finlayson, "The Global Mangrove Watch—A New 2010 Global Baseline of Mangrove Extent," *Remote Sensing*, vol. 10, p. 1669, Oct. 2018. Number: 10 Publisher: Multidisciplinary Digital Publishing Institute.

[41] S. Mulet, M.-H. Rio, H. Etienne, C. Artana, M. Cancet, G. Dibarboure, H. Feng, R. Husson, N. Picot, C. Provost, and P. T. Strub, "The new CNES-CLS18 Global Mean Dynamic Topography,"

[42] S. Muis, M. I. Apecechea, J. Dullaart, J. de Lima Rego, K. S. Madsen, J. Su, K. Yan, and M. Verlaan, "A High-Resolution Global Dataset of Extreme Sea Levels, Tides, and Storm Surges, Including Future Projections," *Frontiers in Marine Science*, vol. 0, p. 263, 4 2020.

[43] R. E. Kopp, R. M. Horton, C. M. Little, J. X. Mitrovica, M. Oppenheimer, D. J. Rasmussen, B. H. Strauss, and C. Tebaldi, "Probabilistic 21st and 22nd century sea-level projections at a global network of tide gauge sites," *Earth's Future*, vol. 2, pp. 383–406, 2014.

[44] R. E. Kopp, R. M. DeConto, D. A. Bader, C. C. Hay, R. M. Horton, S. Kulp, M. Oppenheimer, D. Pollard, and B. H. Strauss, "Evolving Understanding of Antarctic Ice-Sheet Physics and Ambiguity in Probabilistic Sea-Level Projections," *Earth's Future*, vol. 5, pp. 1217–1233, 12 2017.

[45] R. C. Feenstra, R. Inklaar, and M. P. Timmer, "The Next Generation of the Penn World Table," *American Economic Review*, vol. 105, no. 10, pp. 3150–3182, 2015.

[46] World Bank, "International Comparison Program 2017," database, May 2020.

[47] D. Lincke and J. Hinkel, "Coastal Migration due to 21st Century Sea-Level Rise," *Earth's Future*, vol. 9, no. 5, 2021.

[48] R. E. Kopp, A. C. Kemp, K. Bittermann, B. P. Horton, J. P. Donnelly, W. R. Gehrels, C. C. Hay, J. X. Mitrovica, E. D. Morrow, and S. Rahmstorf, "Temperature-driven global sea-level variability in the common era," *Proceedings of the National Academy of Sciences*, vol. 113, no. 11, pp. E1434–E1441, 2016.

[49] G. G. Garner, T. Hermans, R. E. Kopp, A. B. A. Slangen, T. L. Edwards, A. Levermann, S. Nowicki, M. D. Palmer, C. Smith, B. Fox-Kemper, H. T. Hewitt, C. Xiao, G. Aðalgeirsdóttir, S. S. Drijfhout, T. L. Edwards, N. R. Golledge, M. Hemer, G. Krinner, A. Mix, D. Notz, S. Nowicki, I. S. Nurhati, L. Ruiz, J.-B. Sallée, Y. Yu, L. Hua, T. Palmer, and B. Pearson, "IPCC AR6 Sea Level Projections," Aug. 2021. Date Accessed: 01-28-2022. doi:10.5281/zenodo.5914710.